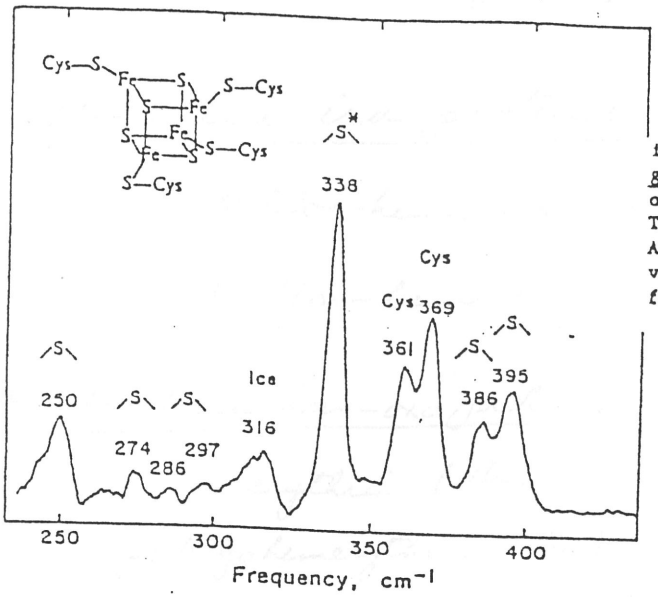

Resonance Raman spectrum of the 4Fe-4S-4Cys cluster in reduced high-potential iron protein from Rhodopseudomonas globiformis. Spectral conditions as in Figure 9, but spectrum of frozen solvent not subtracted out. (From Mino, Y.; Loehr, T. M.; Sanders-Loehr, J.; Cusanovich, M., unpublished results.) Assignments of bridging (-S-) and terminal (Cys) Fe-S vibrations based on S-34 isotope shifts for oxidized ferredoxin from Clostridium pasteurianum (24,43).

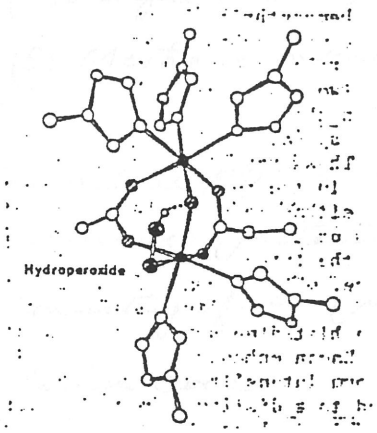

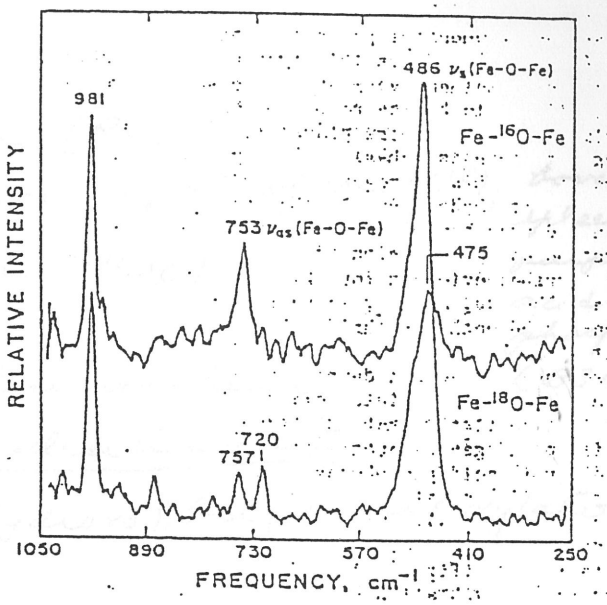

Resonance Raman spectra of oxyhemerythrin with O-16 (upper) and O-18 (lower) in the oxo bridge. Protein (1.2 mM) and Na_2SO_4 (0.3 M) maintained at 5°C in a flow cell and probed with 363.8 nm excitation. (Reproduced from Ref. 34. Copyright 1984 American Chemical Society.)

Table II. Fe-O-Fe Modes in Proteins and Model Compounds[a]

Sample	ν_s(Fe-O-Fe) O-16	[ΔO-18]	{ΔD}	ν_{as}(Fe-O-Fe) O-16	[ΔO-18]
Oxyhemerythrin[b]	486	[-14]	{+4}	753	[-37]
Azidomethemerythrin[b]	507	[-14]	{0}	768	[-35]
Ribonucleotide reductase[c]	492	[-13]	{+3}	756	[-25]
$Fe_2O(Ac)_2(HBpz_3)_2$[d]	528	[-17]		751	[-30]
$[Fe_2O(phen)_4(H_2O)_2]^{4+}$[e]	395	[-5]		827	[-39]

[a]Peak frequencies and isotope shifts in cm^{-1}. [b]Isotope shifts with 18-O in bridge larger than in Figure 4 due to more complete isotope replacement (16). [c]Protein B2, radical-free form (22). [d]Tribridged cluster with tris(1-pyrazolyl)borate capping ligands (31). [e]Monobridged cluster with 1,10-phenanthroline and aquo ligands (32).

CHM 5910 April 6, 1993 Lecture

Non-heme iron proteins

- Non-heme iron-sulfur proteins
- Non-heme iron-oxo proteins

- **Non-heme iron-oxo proteins**

(1) Hemerythrin (Hr)
(2) Myohemerythrin (MHr)
(3) Ribonucleotide reductase (RR)
(4) Purple acid phosphatases (e.g. uteroferrin (Uf); bovine spleen purple acid phosphatase (BSPAP))
(5) Methane monooxygenase (MMO)

→ The active site of each of these non-heme iron-oxo proteins is a binuclear iron unit consisting of a (μ-oxo (or hydroxo))bis(μ-carboxylato) diiron core.

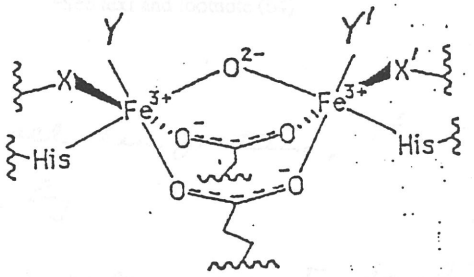

This binuclear unit is readily recognized as a wedge of the basic ferric acetate structure, which consists of a μ_3-oxo triiron core with carboxylates bridging between pairs of iron atoms

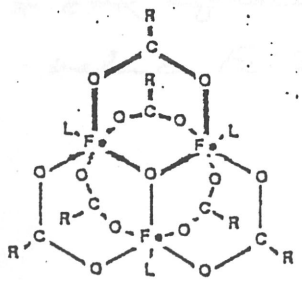

→ Properties of Binuclear Iron-oxo Proteins

Taken from "Metal Clusters in Proteins" (L. Que, Jr. editor) ACS Symposium series Vol. 372 p. 160

Protein	ΔE_Q (mm/s)	J[a] (cm^{-1})	Fe-O,N[b] (Å)	Fe···Fe[b] (Å)
Hemerythrin				
metHrN$_3$ (37,38,28)	1.91		1.78, 2.24[c]	3.25[c]
(31)			1.76, 2.10	3.20
(33)			1.80, 2.13	3.19
(32)			1.80, 2.15	(3.49)
metmyoHrN$_3$ (30)			1.79, 2.16[c]	3.22[c]
metHr (37,38,34)	1.57	-134(χ)		
oxyHr (37,38,34,32)	1.92, 1.00	-77(χ)	1.83, 2.16	(3.57)
metHrCl (38)	2.04			
metHrOH (32)			1.82, 2.15	(3.54)
semimetHrN$_3$ (36,33)		-20(NMR)	1.87, 2.14	3.44
deoxyHr (38,36,47)	2.76	-13±2(χN)	2.02, 2.14[d]	(3.13)
(48)		-25±13(MCD)		
Ribonucleotide reductase				
native (69,60,33,62,69)	1.66, 2.45	-108(χ)	1.79, 2.06	3.22
(63)			1.78, 2.04	3.26[e]
radical free (69,33,62)	1.66, 2.45		1.78, 2.06	3.19
Purple acid phosphatases				
Uf$_o$ (92)	1.65, 2.12			
Uf$_o$-P$_i$ (90,82)	1.02, 1.38		1.96, 2.10[d]	3.2±0.1
Uf$_r$ (92,81,82)	1.78, 2.63	-10(NMR)	2.02, 2.13[d]	3.18
		-7(EPR)		
Uf$_r$-P$_i$ (90)	0.78, 2.76			
BSPAP$_o$-P$_i$ (73,92)		<-150(χ)	1.98, 2.13[d]	3.01
BSPAP$_r$ (73)		-5(EPR)		

[a]J values obtained by fits to variable temperature data obtained by technique indicated. χN denotes a room temperature Evans susceptibility measurement.
[b]Unless noted otherwise, structural parameters are obtained from EXAFS measurements; the shorter distance corresponds to the shortest Fe-O bond and the longer value to the average of 5 longer Fe-O and Fe-N distances. Values in parentheses are considered questionable.
[c]X-ray crystallography. The listed bond lengths were refined without restraints.
[d]The distances corresponds to 3 Fe-O and 3 Fe-N distances per iron.
[e]See text and footnote (64).

→ In all these proteins, the binuclear iron unit is characterized by

* strong antiferromagnetic coupling between the iron centers in their Fe(III) - Fe(III) forms
  $-J > 100\ cm^{-1}$ ($\mathcal{H} = -2J\vec{S}_1 \cdot \vec{S}_2$)
  [the irons are high-spin ($S = 5/2$)]

* EPR ~~signals~~ with $g_{av} \sim 1.7-1.8$ in the mixed valence Fe(II) - Fe(III) forms

→ Antiferromagnetic coupling between two high-spin ferric ions

$$\mathcal{H}_{ex} = -2J\vec{S}_1 \cdot \vec{S}_2$$

$$W_{ex} = -J\left[S_T(S_T+1) - S_1(S_1+1) - S_2(S_2+1)\right]$$

where $S_1 = S_2 = 5/2$; $S_T = S_{total} = 0, 1, 2, 3, 4, 5$

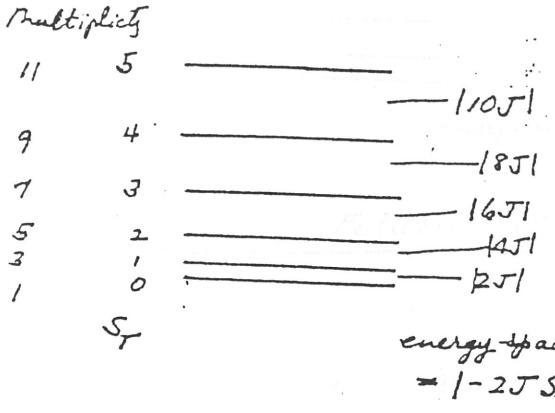

$$\chi^M_{Fe-Fe} = \mu_0 \frac{N_A g^2 \beta^2}{3kT} * \frac{\sum_{S_T=(S_1-S_2)}^{(S_1+S_2)} S_T(S_T+1)(2S_T+1)\, e^{\frac{J(S_T)(S_T+1)}{kT}}}{\sum_{S_T=(S_1-S_2)}^{S_1+S_2} (2S_T+1)\, e^{J(S_T)(S_T+1)/kT}}$$

* Example from Fe-S cluster literature

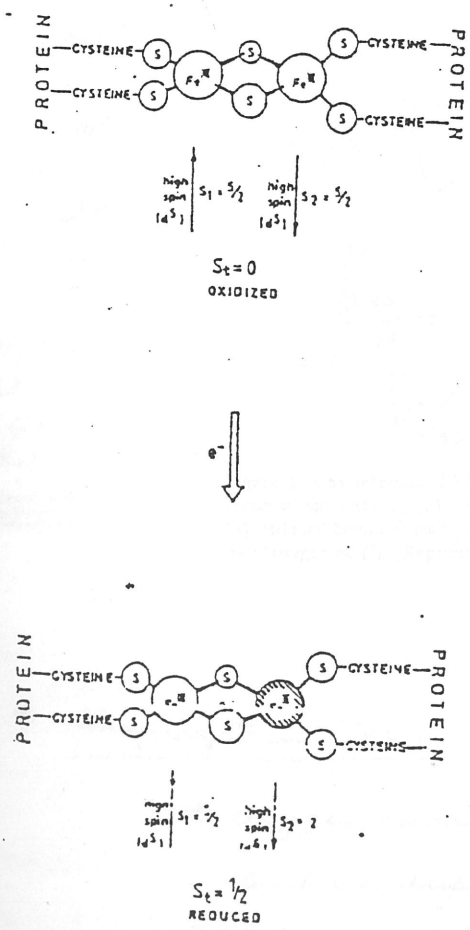

Proposed model for the active center of Fe_2S_2 proteins

Energy diagram for exchange-coupled dimer, $\mathcal{H}_{ex} = -J\vec{S}_1 \cdot \vec{S}_2$, $S_1 = S_2 = 5/2$, $J < 0$. (b) Temperature dependence of the molar susceptibility per iron, χ^M_{Fe}, of $(Ph_4As)_2[Fe_2S_2(S_2\text{-}o\text{-}xyl)_2]$ and calculated curve for $J = -296\ cm^{-1}$. Taken from [78]. Note that χ^M_{Fe} is given in emu $mole^{-1}\ G^{-1}$, which may be transferred into SI-units ($m^3\ mole^{-1}$) by multiplying with $4\pi \times 10^{-6}$. Effective magnetic moments per iron, μ^{eff}, at various temperatures, are calculated from χ^M_{Fe} (in emu $mole^{-1}\ G^{-1}$) using $\mu^{eff} = \sqrt{8\chi^M_{Fe}T}\ \beta$ and from χ^M_{Fe} (in SI-units) using $\mu^{eff} = 797.5\sqrt{\chi^M_{Fe}T}\ \beta$. (c) Dependence of exchange coupling in Fe(III)–Fe(III) dimers from the type of bridges; (*1*): $[Fe_2(edt)_4]^{2-}$ from Herskovitz et al. (1973) Inorg. Chem. 12: 249; (*2*): $[Fe(salen)]_2S$ from Mitchell et al. (1973) J. Inorg. Nucl. Chem. 35: 1385; (*3*): $[Fe_2S_2(S_2\text{-}o\text{-}xyl)_2]^{2-}$ from [78]; (*4*): spinach ferredoxin from Palmer et al. (1971) Biochim. Biophys. Acta 245: 201

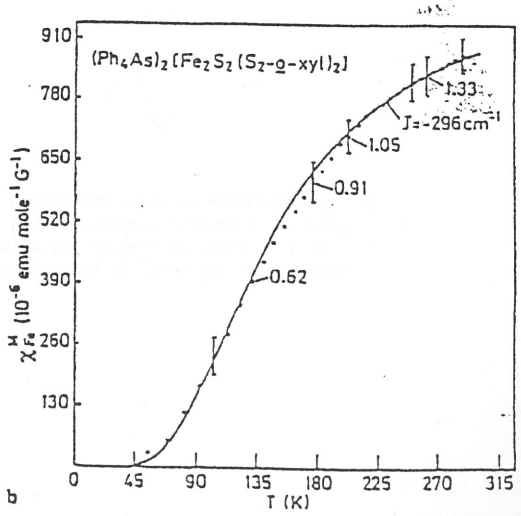

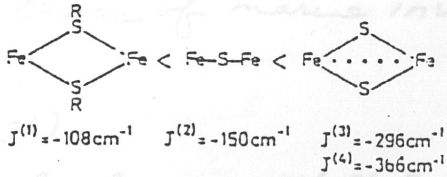

$J^{(1)} = -108\ cm^{-1}$ $J^{(2)} = -150\ cm^{-1}$ $J^{(3)} = -296\ cm^{-1}$ $J^{(4)} = -366\ cm^{-1}$

c

→ Antiferromagnetic interaction between 1 high-spin Ferric ion and 1 high-spin Ferrous ion (mixed valence species)

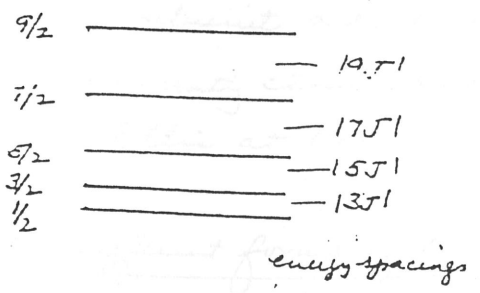

→ EPR of Fe(II)…Fe(III) sites in semimethemerythrin

EPR from $S_T = 1/2$ state

EPR signals disappear above 30K due to accessibility of higher spin state. Therefore coupling (antiferromagnetic) is weak.

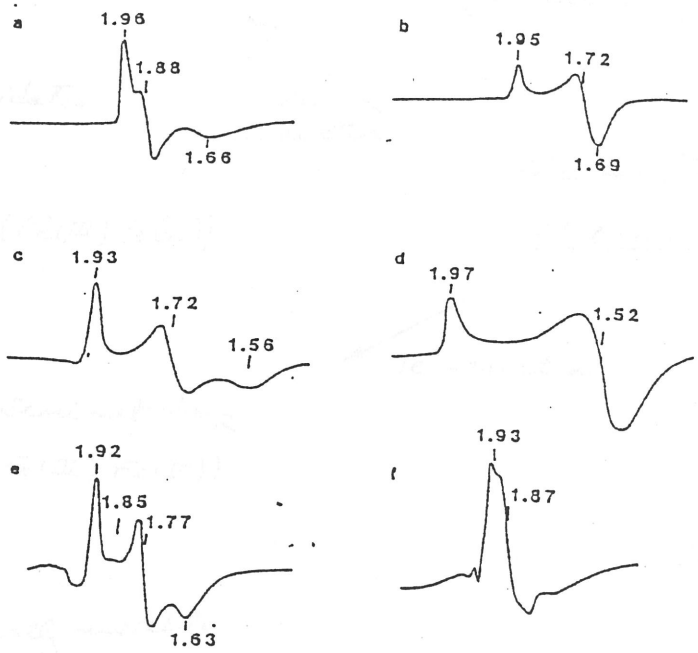

Figure 1. Characteristic EPR signals of Fe(II)Fe(III) sites in semimethemerythrin$_R$ (a), semimethemerythrin$_O$ (b), reduced uteroferrin (c), reduced uteroferrin-molybdate complex (d), reduced bovine spleen purple acid phosphatase (e), reduced component A of methane monooxygenase (f). (Reproduced with permission from ref. 26. Copyright 1987 Elsevier.)

Two semimetHr forms: semimetHr$_O$ and semimetHr$_R$

- Hemerythrin (Hr)

→ Oxygen carrier from a class of marine invertebrates such as sipunculids

→ subunit structure : $(\alpha)_n$

molecular mass of $\alpha \equiv 13$ kDa

→ Each α subunit contains a binuclear Fe oxo unit

that binds O_2 reversibly (1 molecule of O_2 per 2 irons)

→ <u>Myohemerythrin</u> (MHr) from worm has only 1 subunit and 1 binuclear iron oxo unit (recently cloned and overexpressed by Walter Ellis at Univ. of Utah)

→ <u>Different forms of the protein</u>

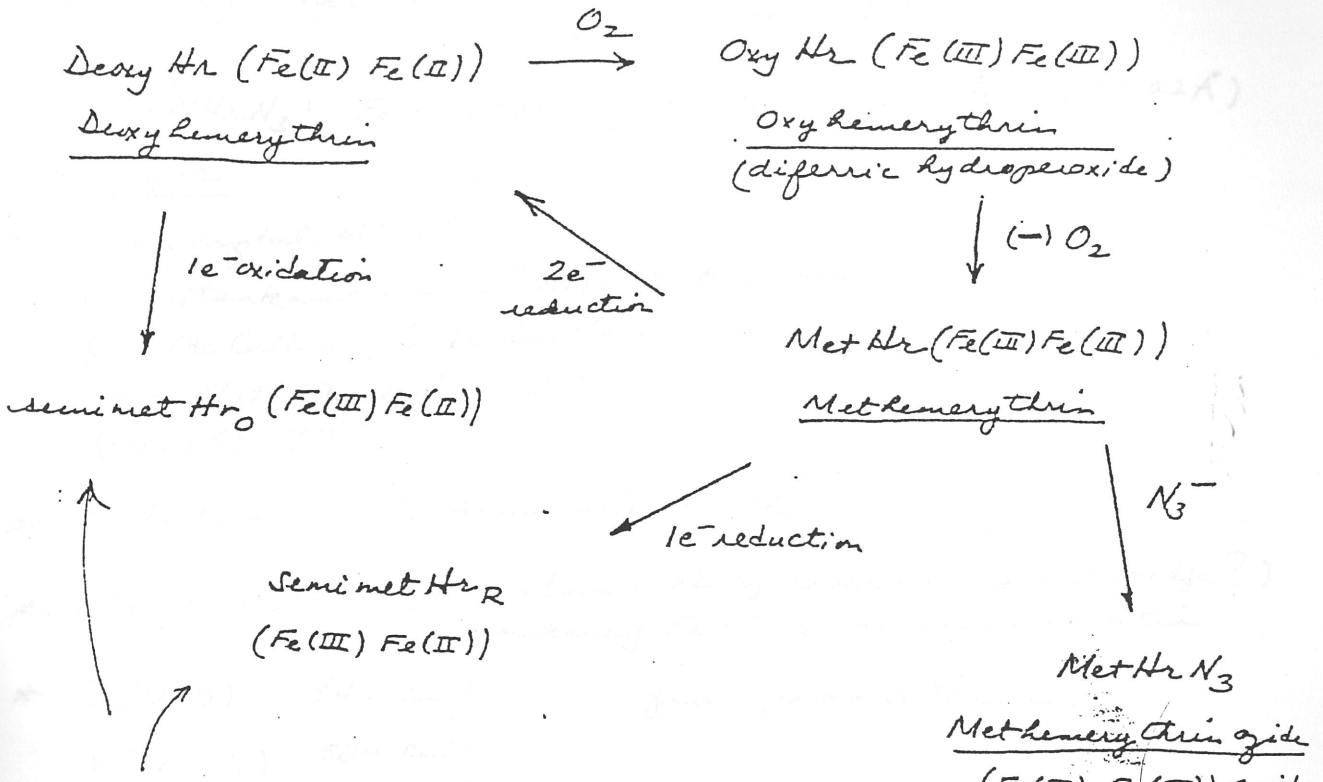

kinetic "stability" of semimethemerythrins due to conformational change that occurs between the deoxy and met states of the protein

→ <u>Met Hr N_3</u> & <u>Met M Hr N_3</u>

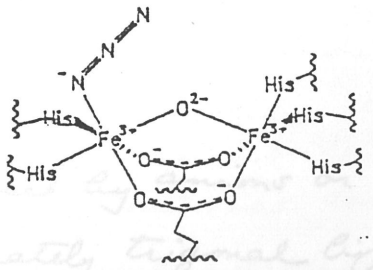

metHrN3

* X-ray crystal structure (Met Hr N_3)
R.E. Stenkamp, L.C. Sieker and L.H. Jensen
J. Am. Chem. Soc. (1984) <u>106</u>, 618–622

<u>Met M Hr N_3</u>: S. Sheriff, W.A. Hendrickson and J.L. Smith, J. Mol. Biol. <u>197</u>, 273–296 (1987).

* Iron centers are bridged by an <u>oxo</u> group with Fe–O bond lengths averaging 1.76 Å
  Fe–N 2.24 Å
* Carboxylates from <u>one</u> aspartate and <u>one</u> glutamate
* Remaining coordination sites are occupied by five Histidines and the azide.
* Azide binds end-on.
* Fe(III) ··· Fe(III) distances 3.25 Å (X-ray)
  3.20 Å (EXAFS)
* MetMHbN$_3$: Fe–O (1.79 Å); Fe–N (2.16 Å); Fe···Fe (3.22 Å)

→ <u>OxyHb</u>

* X-ray crystal structure
  R. E. Stenkamp, L. C. Sieker, L. H. Jensen
  J. D. McCallum, J. Sanderi-Loehr
  Proc. Natl. Acad. Sci. USA
  (1985) <u>82</u>, 713-716.
* O_2 binds end-on to same site as N_3^-
* $J = -77\ cm^{-1}$ (hydrogen-bonding of hydroperoxide to oxo bridge?) weakening Fe–O–Fe exchange interaction
* ν(O–O) 844 cm^{-1} from Resonance Raman
  ν(Fe–O_2) 504 cm^{-1}
  ↖ stretches
* $^{18}O_2$ and $^{16}O\,^{18}O$ experiments indicate that O_2 binds as a monodentate ligand
* Stretching frequencies change in D_2O, indicating that O_2 is bound as hydroperoxide

→ <u>MetHb</u>

* Coordination site normally occupied by anions or O_2 vacant, so one iron is approximately trigonal bipyramidal.

* $J = -134\ cm^{-1}$

* Fe–μ–O bond length ~ 1.8Å (EXAFS)
  Fe ··· Fe distance ~ 3.2Å (EXAFS)

* Resonance Raman bands
  506–514 cm^{-1} ν_s of Fe–O–Fe unit
  750–780 cm^{-1} ν_{as} of Fe–O–Fe unit

→ <u>Deoxy Hr</u>

* Triply bridged core structure retained.

* A low (3.9Å) resolution difference electron density map of deoxy Hr <u>vs</u> met Hr from X-ray diffraction suggests that the iron atoms move slightly further apart in deoxy Hr, but remain five- and six-coordinate, respectively
  Fe–O distance 2.02Å (from EXAFS)
  Fe–N distance 2.14Å (from EXAFS)

* Fe(II) ··· Fe(II) weakly coupled only
  $J = -15\ cm^{-1}$ (antiferromagnetic)
  Comparison of X with model compounds suggests that <u>oxo</u> group in <u>met Hr</u> can become protonated in deoxy Hr

* Binding of anions to deoxy Hr alters the properties of binuclear unit. Dioxygen binding is retarded by the presence of azide, cyanate, or fluoride. Also magnetic properties are altered, indicating changes in bridging groups.

Taken together, the physical evidence suggests that deoxy Hr contains a (μ-hydroxo) bis (μ-carboxylato) diferrous core.

Upon binding anions, the hydroxo group may either be protonated or become non-bridging, either of which would account for the loss of antiferromagnetic coupling in deoxy HrX.

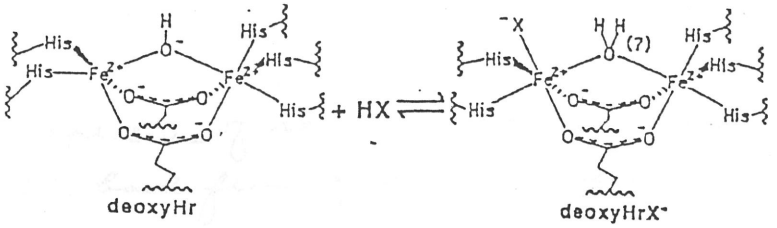

Semimet Hr's

(Semimet Hr_O and Semimet Hr_R)

* thermodynamically unstable intermediates in the oxidation of deoxy Hr or reduction of met Hr

* Two forms of semimet Hr are generated depending on whether deoxy Hr is oxidized (to generate semimet Hr_O) or met Hr is reduced (to generate semimet Hr_R)

* Both forms exhibit distinct EPR signals with $g_{av} \sim 1.8$ indicative of antiferromagnetic coupling between Fe(II) and Fe(III) centers)

* Coupling is weak $J = -20\ cm^{-1}$. EPR disappears above 30K.

* Both semimet Hr bind anions and give the same anion complex, which is more stable, irrespective of whether the semimet Hr_O or semimet Hr_R is used to prepare anion adduct. Spectroscopic evidence favors a μ-hydroxo bridge for semi Met HrX, with X^- bound to the ferric ion

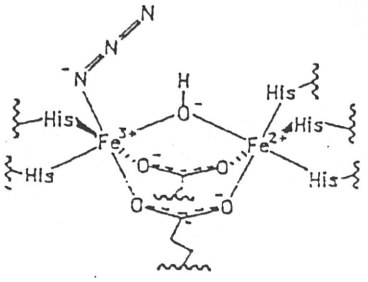

* visible spectrum of semimet Hr N_3 shows a charge transfer band from azide to the ferric ion at 470 nm. Similar band at 446 nm in met Hr N_3.

→ <u>Mechanism of oxygen binding to hemerythrin</u>

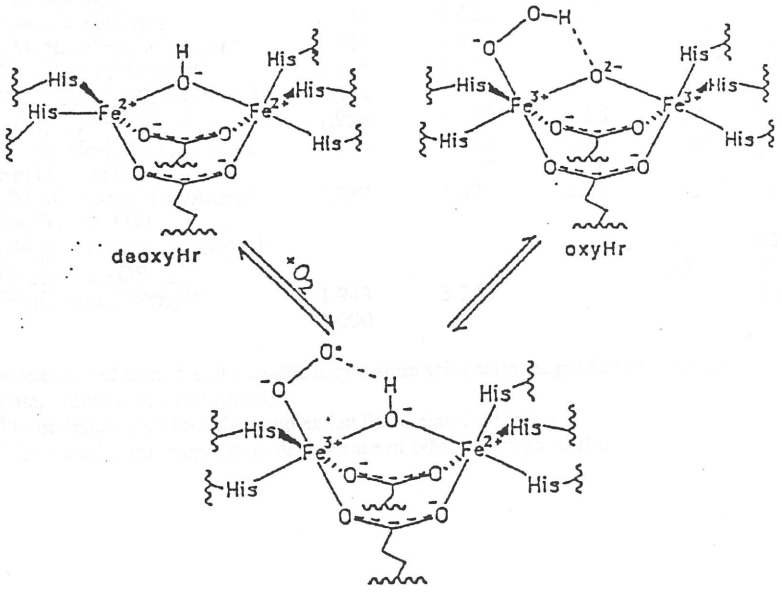

Facile & reversible : RX requires minimal rearrangement and no high-energy intermediate

→ <u>Synthetic Analogues of Hr</u>

The thermodynamic stability of the Hr binuclear core has recently been demonstrated by the spontaneous assembly of the core structure with a number of trigonal capping

ligands.

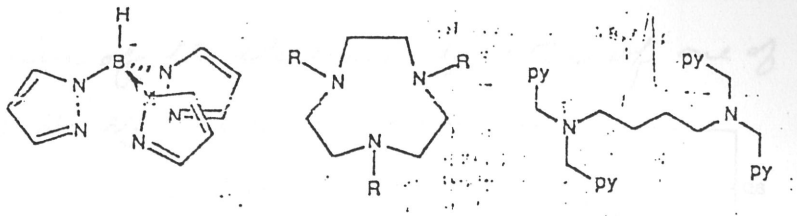

1, $HBpz_3$ 2, tacn (R=H) 3, Me_3tacn (R=Me) 4, tpbn

Table I. Comparison of Structural and Spectroscopic Parameters of Binuclear Iron Complexes

Complex	$r_{Fe-\mu-O(R)}$ (Å)	$r_{Fe\cdots Fe}$ (Å)	ΔE_Q (mm/s)	J[a] (cm^{-1})	Ref
Fe(III)-Fe(III)					
$[(HBpz_3Fe)_2O(OAc)_2]$	1.784	3.146	1.60	-121	5
$(HBpz_3Fe)_2O(O_2CH)_2]$	1.781	3.168			5
$[(tacnFe)_2O(OAc)_2]^{++}$	1.781	3.063	1.72		6
$[(Me_3tacnFe)_2O(OAc)_2]^{++}$	1.800	3.12	1.50	-119	8
$[tbpnFe_2O(OAc)_2]_2^{4+}$	1.794	3.129	1.27	-120[b]	9
$[(HBpz_3Fe)_2O(O_2P(OPh)_2)_2]$	1.808	3.337		-98	13
$[(HBpz_3Fe)_2OH(OAc)_2]^+$	1.956	3.439	0.25	-17	18
$[Fe_2(5\text{-Me-HXTA})(OAc)_2]^-$	2.008	3.442	0.58	-10[c]	19
Fe(II)-Fe(II)					
$[(Me_3tacnFe)_2OH(OAc)_2]^+$	1.987	3.32	2.83	-13	8
Fe(II)-Fe(III)					
$[Fe_2(5\text{-Me-HXTA})(OAc)_2]^{2-}$				-5[c]	23
$[Fe_2(bbmp)(OBz)_2]^{2+}$				-5	24
$[Fe_2(bpmp)(OPr)_2]^{2+}$	1.943 2.090	3.365			22

[a]Determined from fits of variable temperature solid state magnetic susceptibility data, unless otherwise noted.
[b]J not determined for this complex but for a related complex.
[c]Estimated from temperature dependence of NMR isotropic shifts

* $Fe-O_{oxo}$ bond length of 1.78-1.80Å

Carboxylate bridges restrict Fe-O-Fe angle to ~ 120° ± 10°

& the Fe... Fe distance to 3.15 ± 0.1Å

* <u>Electronic spectra</u>: a strong (ϵ ~ 3000-4000 $M^{-1}cm^{-1}$) absorption at 300-400 nm with a characteristic shoulder both associated with presence of oxo-bridge; weaker (ϵ ~ 300-600 $M^{-1}cm^{-1}$) features in the 400-550 nm associated with (μ-oxo) bis(μ-carboxylato)-diferric

the visible and near UV bands result in the observation of enhanced Raman bands due to Fe–O–Fe vibrations.

* A comparison of the electronic spectra of one of the models (Fe(III)–Fe(III)) with MetHr N_3

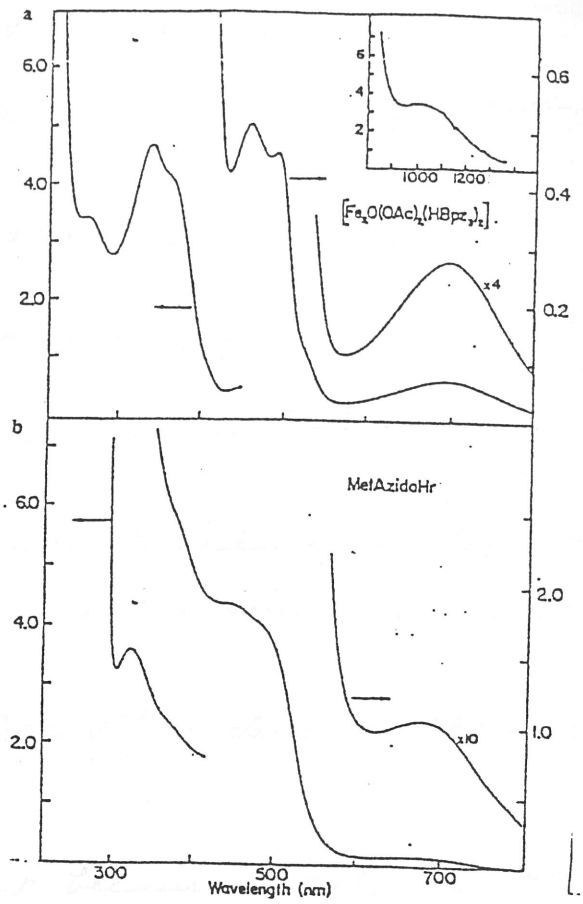

Electronic spectra of $[(HBpz_3Fe)_2O(OAc)_2]$ (a) and methemerythrin azide (b). The y-axis units are for ϵ_{Fe} in $cm^{-1}mM^{-1}/Fe$. (Reproduced from ref. 5. Copyright 1984 American Chemical Society.)

* The oxo group of the model compound $[(HBpz_3Fe)_2O(OAc)_2]$ can be protonated by HBF_4 to yield $[(HBpz_3Fe)_2OH(OAc)_2]$

Protonation lengthens Fe–μ–O bond to 1.96Å
increases Fe···Fe separation
decreases Fe–O–Fe angle
decreases antiferromagnetic coupling to $J \simeq -17$ cm^{-1}

* Only ~~one~~ Fe(II)...Fe(II) known

$[(Me_3tacn\ Fe)_2OH(OAc)_2]^+$

Fe–μOH	1.99Å
Fe···Fe	3.4Å
J	$-13\ cm^{-1}$.

Cytochrome c Oxidase — what it does

- Redox-linked proton pump
- Redox-energy derived from the following reaction

$$4\ \text{Ferrocytochrome c} + O_2 + 4H^+ \longrightarrow 4\ \text{Ferricytochrome c} + 2H_2O$$

Reaction is mediated by this enzyme.

- $4e^-$ are required to reduce one O_2 molecule; $4H^+$ are consumed per turnover. $\Delta G^{o\prime} \cong -50$ kcal/mole O_2 reduced
- Turnover Number ~ $400\ s^{-1}$; Dioxygen chemistry is facile
- Enzyme important because >90% O_2 we breathe is consumed by the above reaction.
- Enzyme is interesting, because it is a molecular machine, a free energy transducer that converts redox energy to H^+ electrochemical potential. In this manner, part of the free energy is conserved. The enzyme attempts to run this reaction under as reversible conditions as possible while ensuring a reasonable rate. Thermodynamic efficiency ~ 50%.
- This chemistry takes place in the inner membrane of the mitochondrion
- To accomplish this chemistry, the enzyme exploits the

sidedness of a membrane. The enzyme is a membrane protein and it mediates two distinct reactions:

(1) Charge separation

a) electrons from ferrocytochrome c enter the oxidase from one side of the membrane

b) protons consumed in the dioxygen chemistry are taken up from the other side of the membrane.

This charge separation is called the SCALAR reaction

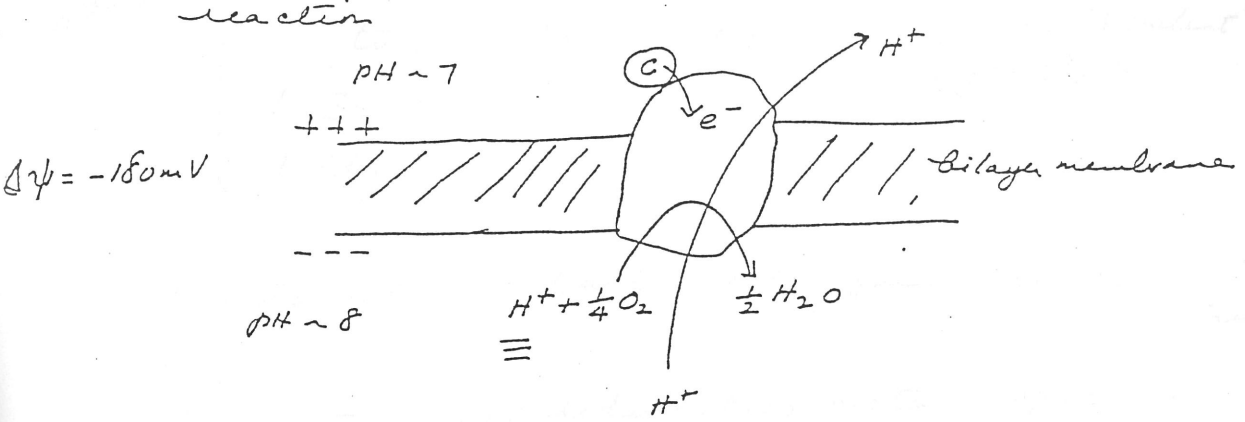

(2) Proton pumping

Enzyme is an electrogenic proton pump, capable of pumping up to 4 H^+ per molecule of O_2 reduced against the H^+ electrochemical potential

$(H^+/e^-)_{average} \sim 1$

What we know about its structure

- Number of subunits

Mammalia (eucaryotes) — 13 subunits — molecular mass ~ 200K

lower eucaryotes: Yeast, Neurospora crassa (fungal) — 13 subunits

prokaryotes: Bacterial
Thermophilic bacillus PS3 : 4
Paracoccus denitrificans : 2 or 3

T. thermophilus caa_3 : 1
ba_3 : 2
aa_3 : 2

Minimum # of subunits for functioning enzyme : 2

- <u>Metalloprotein</u>

Mammalian enzyme
- 2 heme <u>A</u>
- 2 redox active copper
- 1 additional copper (does not appear to be redox active) — part of a mixed valent binuclear copper cluster
- 1 Zn
- 1 Mg

No Zn or Mg in bacterial enzyme, but Mn^{2+} in Paracoccus denitificans

- <u>Ligand structure of redox active metal cofactors</u>

(1) $\boxed{\text{Cytochrome } \underline{a}}$ his N Fe$^{+3/+2}$ N his — six-coordinate bis-imidazole heme A

often referred to as <u>low</u> potential cytochrome.

<u>Redox potential</u> ~ +380 mV when all metal centers are oxidized
~ 250 mV otherwise

(2) $\boxed{\text{cytochrome } \underline{a_3}}$ his N Fe$^{+3/+2}$ ··· L — five- or six coordinate high-spin heme A with imidazole nitrogen of histidine as fifth ligand in <u>native</u> enzyme

(3) $\boxed{Cu_A^{1+/2+}}$
2 histidine nitrogens and 2 cysteine sulfurs

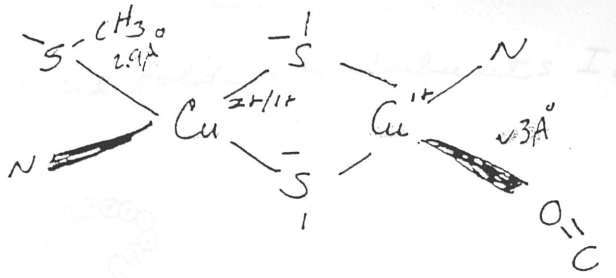

Redoxpotential ~ 270 mV

(4) $\boxed{Cu_B^{1+/2+}}$

3 histidine nitrogens

Redoxpotential ~ 340 mV in oxidized enzyme

- Location of metal cofactors

Subunit I : Cytochrome a, a_3 ; Cu_B

Subunit II : Cu_A

interface { Subunit I / Subunit II: Mg } mammalian

Subunit IV a, b : Zn

- Function of metallic cofactors

Cytochrome a, Cu_A : intercept electrons from Cytochrome c

Cytochrome a_3, Cu_B : catalyzes dioxygen chemistry

Mg : [redacted] ? conformational transition

- Primary sequence of polypeptides

→ Known for many species

→ Ligands to metal sites all conserved from species to species.

→ Proposed folding of subunits I, II and III

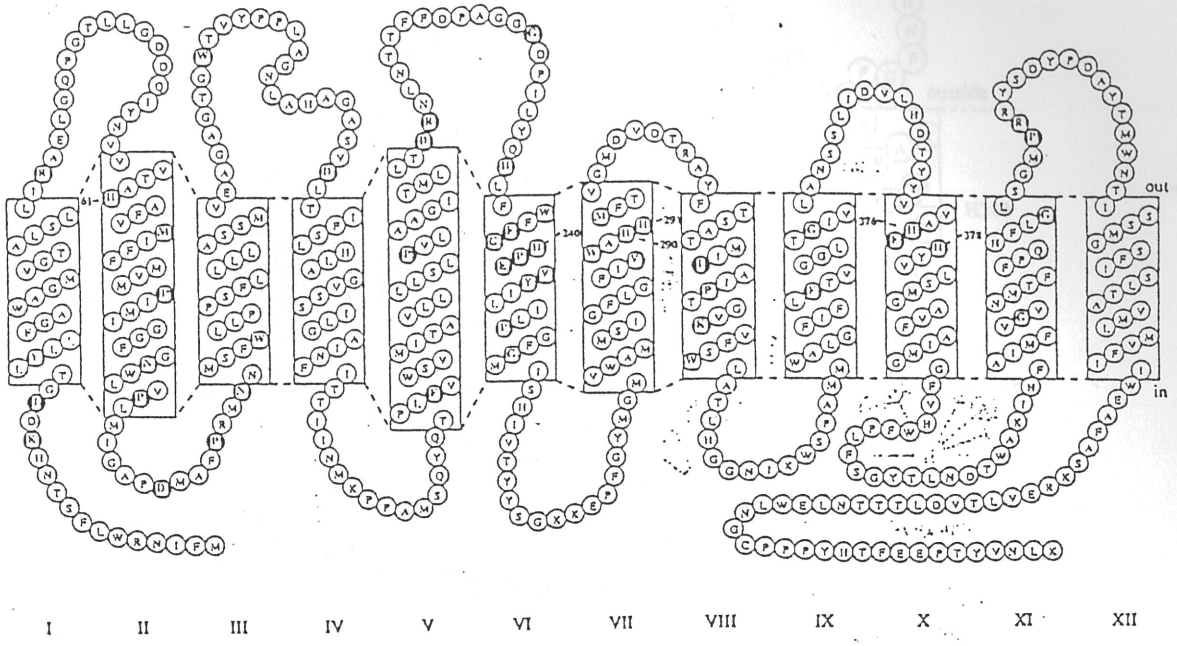

I

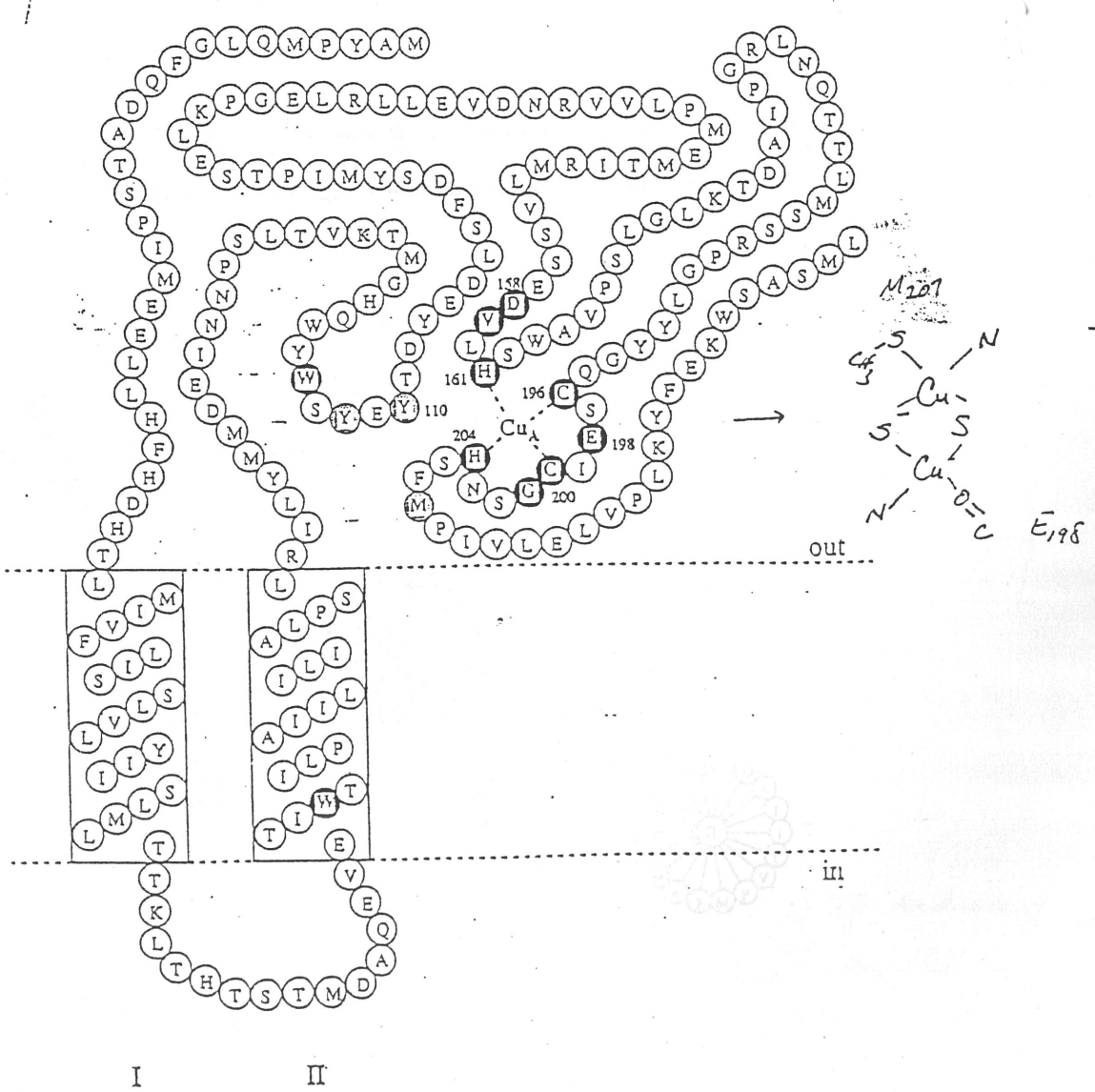

II

ins-membrane α-helices

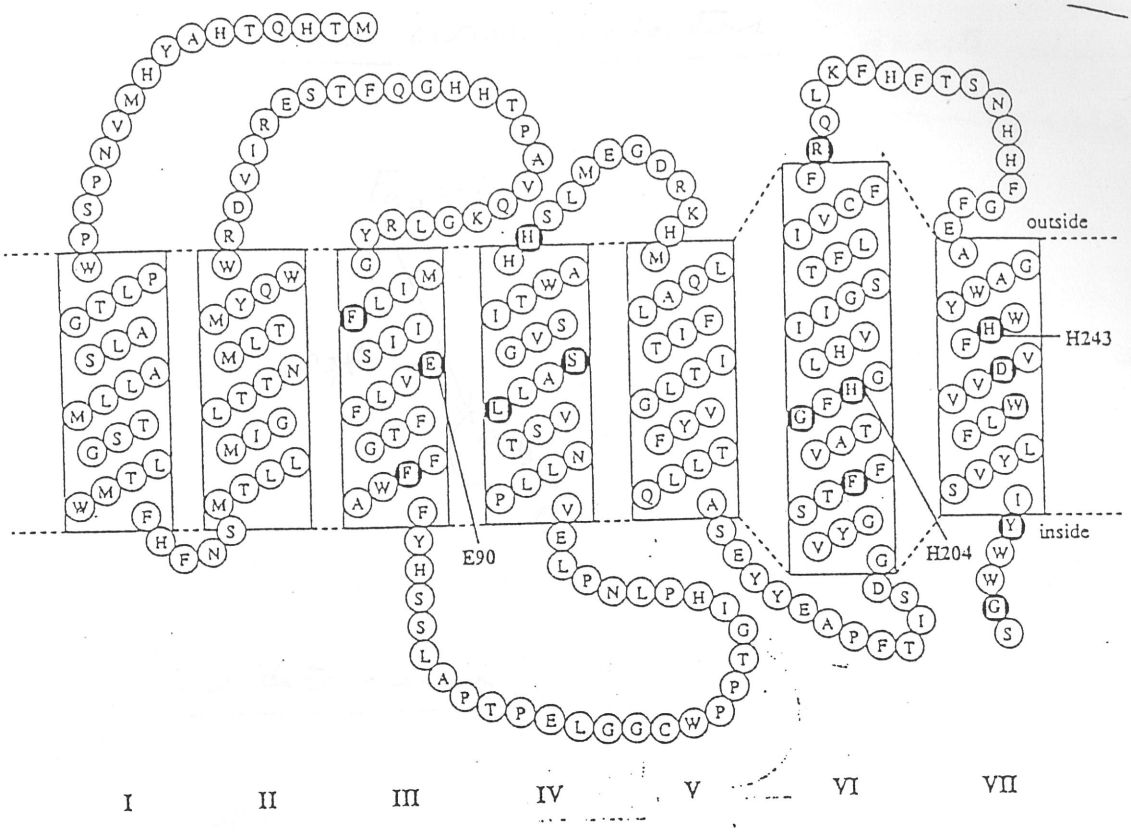

III

→ The ligands of heme a, heme a_3 and Cu_B from site-directed mutagenesis studies

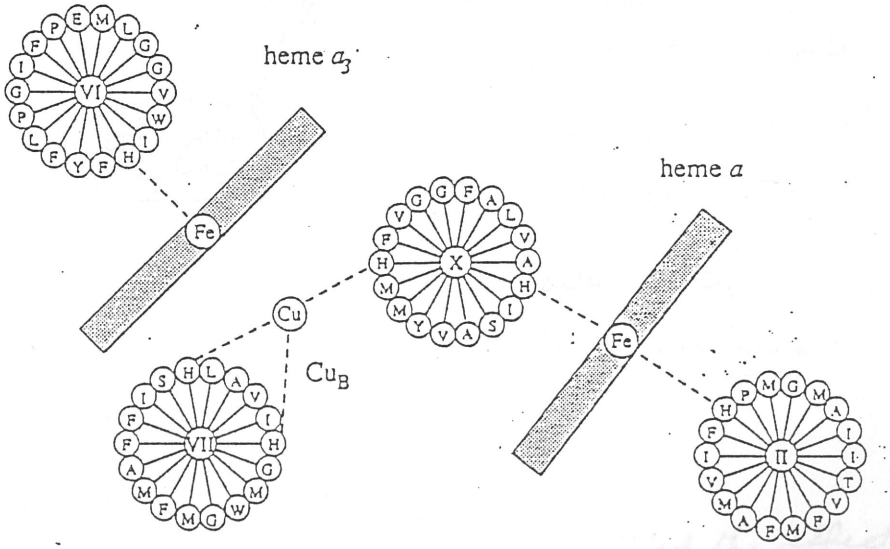

- <u>Distance between cofactors</u>

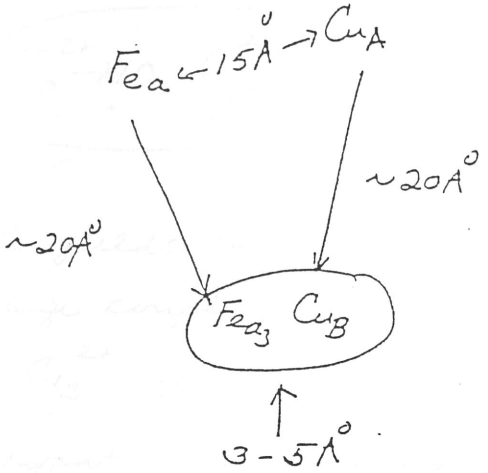

<u>How determined?</u>

a) $Fe_a^{3+/2+} \longleftrightarrow Cu_A^{2+}$

studied the effect of reducing Fe_a on the electron-spin relaxation behavior of $\boxed{Cu_A^{2+}}$

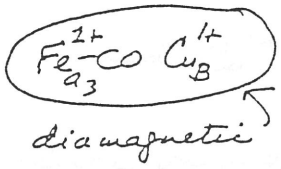

b) Fe_a^{2+} Cu_A^{2+}

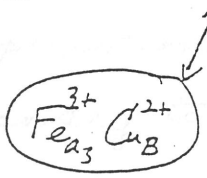

studied the effect of antiferromagnetic coupled $Fe_{a_3}^{3+}$ Cu_B^{2+} (S=2) on the electron-spin relaxation behavior of $\boxed{Cu_A^{2+}}$ when Fe_a^{2+} is reduced (diamagnetic)

c) $Fe_a^{3+/2+}$ $Cu_A^{2+/1+}$

$\updownarrow$

$Fe_{a_3}^{2+}$-NO Cu_B^{1+}

studied the effect of reducing Fe_a^{3+} and Cu_A^{2+} on the electron spin relaxation behavior of NO bound to $Fe_{a_3}^{2+}$ Cu_B^{1+}

(d) Fe_a^{3+} Cu_A^{2+}

one-quarter-reduced NO-bound ferrocytochrome a_3

$Fe_{a_3}^{2+}$–NO Cu_B^{2+}

Cluster yields a triplet state EPR signal due to exchange coupling between NO bound to heme A and Cu_B^{2+} spin (see next page for triplet state EPR)

<u>Two important conclusions</u>

(1) histidine imidazole (fifth ligand) <u>distal</u> to Cu_B
Therefore NO, CO and O_2 binding pocket on the <u>same</u> side as Cu_B^{2+}

(2) Zero-field splitting observed for the triplet
→ a distance of 3.5Å between NO spin and Cu^{2+} spin. $|D| \cong 0.07\ cm^{-1}$

To produce one-quarter-reduced nitrosyl ferrocytochrome $a_3 \cdot Cu_B^{2+}$ complex, the high reduction potential of cytochrome a_3 was exploited to activate the disproportionation of N_3^- in the presence of NO according to the overall reaction:

ferricytochrome a_3 + N_3^- + 2NO ⟶
nitrosyl ferrocytochrome a_3 + N_2 + N_2O

Re: T.H. Stevens <u>et al</u> Proc. Natl. Acad Sci. USA <u>76</u> 3320 (1979).

- Crystals of cytochrome c oxidase and structures of the proteins have been reported (bovine, paracoccus dinitrificans) Science 1996, 199. Nature 1996

What we know about how it works

At least 4 parts to this problem

(1) Dioxygen Chemistry (driving force)

(2) Electron Transfer Pathways (control electron leaks + redox-linkage)

(3) Redox-linkage (moving proton across osmotic barrier)

(4) Regulation and Control (in response to ATP levels, $\Delta\Psi$, ΔpH)

(A) Dioxygen Chemistry

- Dioxygen Chemistry is important because

→ no free energy transduction (charge separation + proton pumping) without dioxygen chemistry

→ protons are pumped only when electrons are transferred to dioxygen reduction intermediates anchored at binuclear cluster

→ protons are not pumped when electrons are transferred to the unloaded dioxygen-reduction site (insufficient driving force)

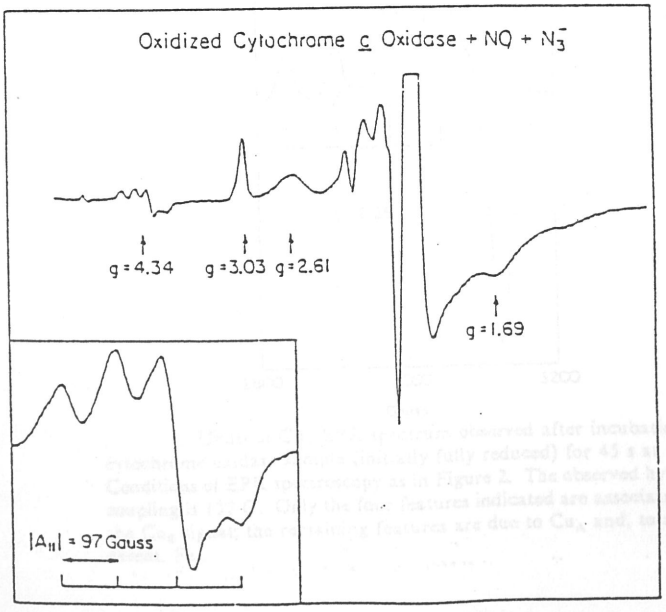

X-band EPR spectrum of the nitrosylferrocytochrome a_3, Cu_B(II) species at 7 K. (Inset): Magnified view of the half-field transition region.

triplet EPR - half-field transition ($\Delta m_S = \pm 2$)

Dioxygen Chemistry at low temperatures

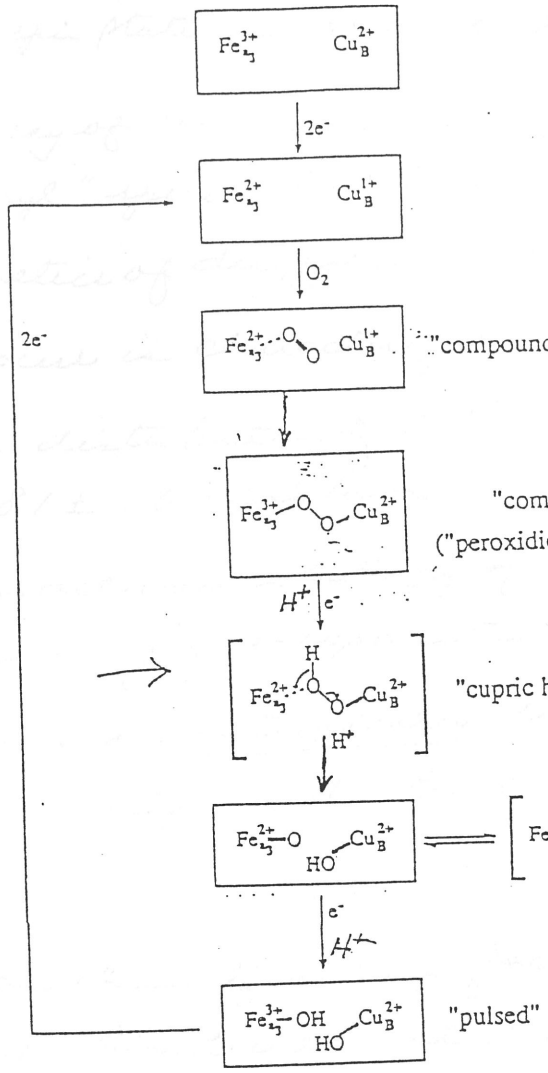

λmax ~ 607 nm
Redox potential
≅ 800 mV

λmax
~580 nm
Redox
potentia
≅ 940 mV

usual
EPR
with $g_{\parallel}$ ~ 2.26
and $A_{\parallel}$ ~137 Gauss
but ⊥
components
are not
resolved;
also unlike
the 2 copper sites,
this EPR signal
is not saturable

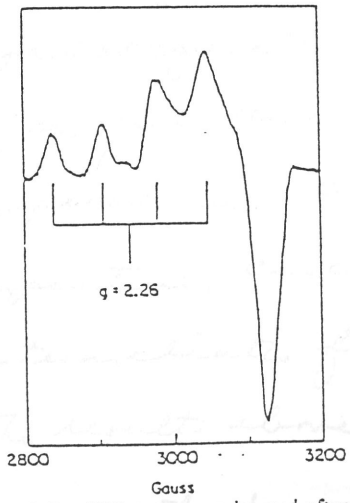

Unusual Cu_B EPR spectrum observed after incubation of a cytochrome oxidase sample (initially fully reduced) for 45 s at 191 K. Conditions of EPR spectroscopy as in Figure 2. The observed hyperfine coupling is 137 G. Only the four features indicated are associated with the Cu_B signal; the remaining features are due to Cu_A and, to a lesser extent, Fe_a.

Ref.
D.F. Blair, S.N. Witt
and S. I. Chan
J. Am. Chem. Soc.
107, 7389 (1985)

→ Unusual Cu_B EPR signal due to coupling of Cu_B^{2+} d^9 hole with ferrous ion in intermediate spin state or high spin state via weak exchange interaction

→ The decay of the "Cupric hydroperoxide" to the "oxyferryl" species has been studied by following the kinetics of disappearance of the unusual Cu_B EPR. The process is characterized by

* a distribution of $\Delta H^{\ddagger}$'s which peaks at 18.1 ± 1.6 kcal/mol
* an activation entropy of $+21.4 \pm 8.2$ cal/mol assuming pre-exponential factor of 10^{13}

So process is <u>entropically</u> driven, indicating that this step is the bond cleavage or scission step.

→ Dioxygen chemistry is very facile under ambient conditions. Bimolecular rate constant for combination of reduced enzyme with O_2 is 8×10^6 $M^{-1} s^{-1}$ at room temperature. So, in order to look at intermediates, need to <u>look</u> (spectroscopically) very quickly, say $10^{-6} - 10^{-3}$ sec, or slow down the reaction by going down to low temperatures. In the latter case, by controlling the temperature, can control electron transfer and even <u>trap</u> intermediates for spectroscopic observations. The results above were obtained by the <u>low temperature method</u>.

* (1) The enzyme is reduced and then inhibited by carbon monoxide in the dark (CO-adduct is photolabile)

$$\boxed{Fe_{a_3}^{2+} \quad Cu_B^{1+}} \longrightarrow \boxed{Fe_{a_3}^{2+}-CO \quad Cu_B^{1+}}$$

(ii) O_2 is rapidly stirred into the solution at ~ 250K. Under these conditions, dissociation of CO from $Fe_{a_3}^{2+}$ very slow, and reoxidation of enzyme by O_2 does not occur.

(iii) The mixture is then frozen at 77K. To initiate dioxygen chemistry, the sample is irradiated with visible light to photodissociate CO. When sample is then warmed to ~160K, dioxygen chemistry occurs

$$Fe_{a_3}^{2+}-CO \quad Cu_B^{1+} \xrightarrow[77K]{h\nu} Fe_{a_3}^{2+} \quad Cu_B^{1+}$$

$$\downarrow >160K \quad O_2$$

$$\leftarrow \leftarrow \leftarrow Fe_{a_3}^{2+}\cdots O_2 \quad Cu_B^{1+}$$

→ Important conclusions from this study

(i) Two dioxygen-reduced intermediates at the $3e^-$ level of reduction

(ii) O_2-bond is cleaved at the three-electron level of reduction, as in Cytochrome P-450 (and peroxidases) and laccase.

(iii) Electron transfers from low potential centers (Fe_a^{2+} and Cu_A^{1+})

<u>Heterogeneous</u> (artifact of starting with $4e^-$ in protein!)

3rd electron to O_2	can come from either	Cu_A^{1+} or	Fe_a^{2+}
4th electron	then comes from	Fe_a^{2+} or	Cu_A^{1+}
<u>Branching ratio</u> at 181K		70%	30% faster branch

Dioxygen Chemistry at Room Temperature

→ Chemistry is much faster; must appeal to time-resolved spectroscopy (sub-microsec → millisec)

(i) Transient absorption spectroscopy
(exploiting the effects of redox on λ_{max} & ϵ of metal centers)

heme $\underline{a}^{3+/2+}$ 605 nm (α-band)

heme $\underline{a_3}^{3+/2+}$ Soret absorption

$Cu_A^{2+/1+}$ 830 nm

(ii) Time-resolved Raman (resonance) spectroscopy

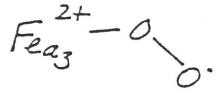

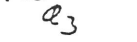

→ Same dioxygen intermediates are formed

(i) O_2 adduct (Compound A)

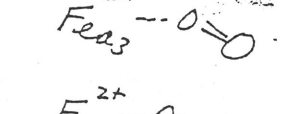

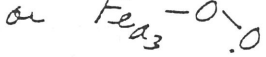

(ii) Peroxo-intermediate (Compound P or Compound C)

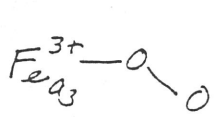

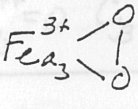

(iii) Oxyferryl intermediate (Compound F or B)

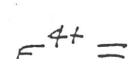

O–O bond is cleaved at the 3-electron level of reduction

→ Electron transfer reactions in the single-turnover experiment under ambient conditions is also <u>heterogeneous</u>!

<u>Kinetic outcome</u> of the single-turnover experiment depends on whether the <u>second electron</u> to the dioxygen originates from Cu_B^{1+} or (Fe_a^{2+} or Cu_A^{1+})

<u>Second electron</u>

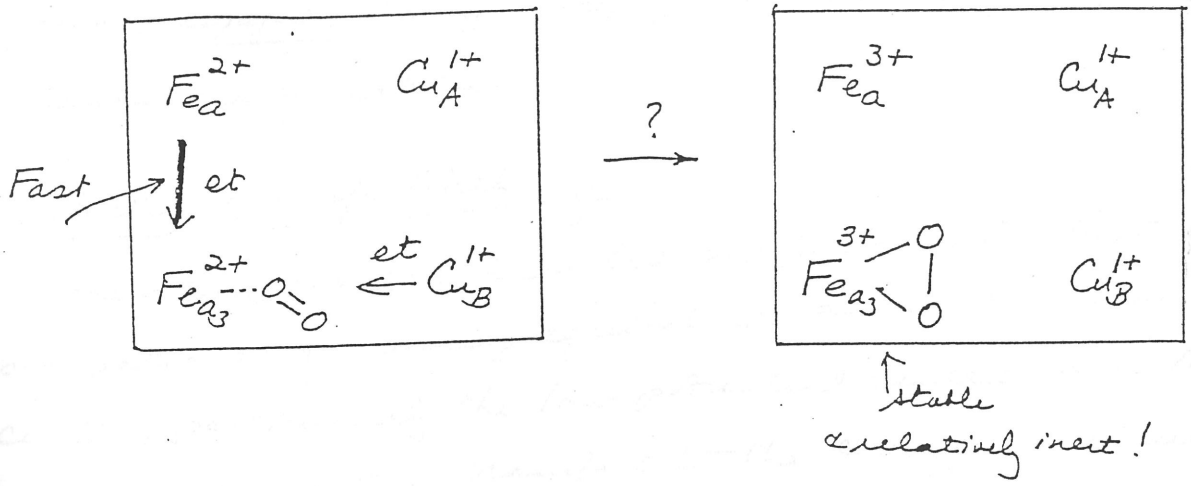

<u>Third electron</u>

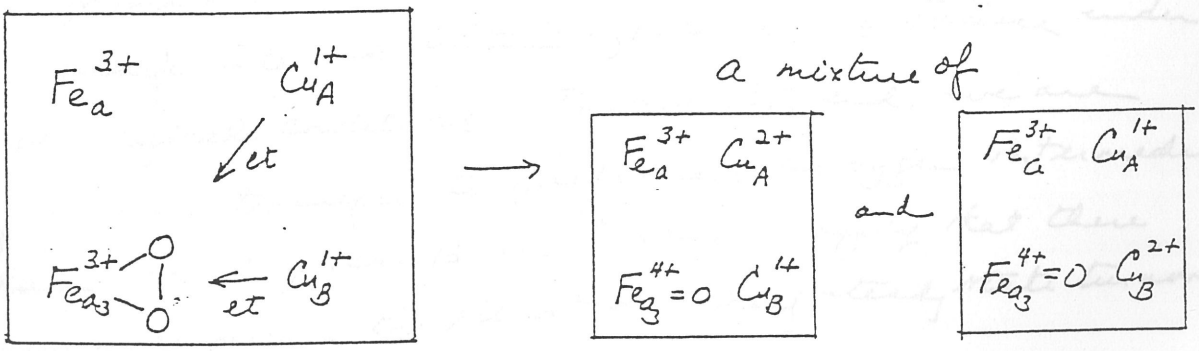

<u>Conclusion</u> Fully reduced enzyme cannot be physiological; i.e., Uncoupling pathways become <u>populated</u> when all four metal "Electron leaks" centers in the enzyme are <u>initially</u> reduced.

Best evidence in support of this conclusion

T. Nilsson, S. Hallen and M. Oliveberg, FEBS Letters 260, 45–47 (1990); M. Oliveberg, S. Hallen and T. Nilsson, Biochemistry 30, 436–440 (1991)

This group studied rapid proton release during flash-induced oxidation of fully reduced oxidase reconstituted into vesicles and obtained evidence for only 1–2 H^+ per turnover. (Versus $4H^+$/turnover). Thus, the proton pumping machinery is not engaged during much of the turnover cycle, i.e., electron leaks are generative.

(B) Electron Transfer Pathways

The above results have led us to surmise that the occupation # of reducing equivalents among the redox centers, particularly the low potential centers, and the sequence of electron transfers to the dioxygen molecule is crucial to the engaging of the proton pumping machinery. This has prompted us to develop methods to study the electron transfer into and within cytochrome c oxidase under more physiological conditions. Toward this end, we are studying electron transfer to preformed dioxygen intermediates that have been implicated in turnover, hoping that these conditions will mimic the situation during steady state turnover.

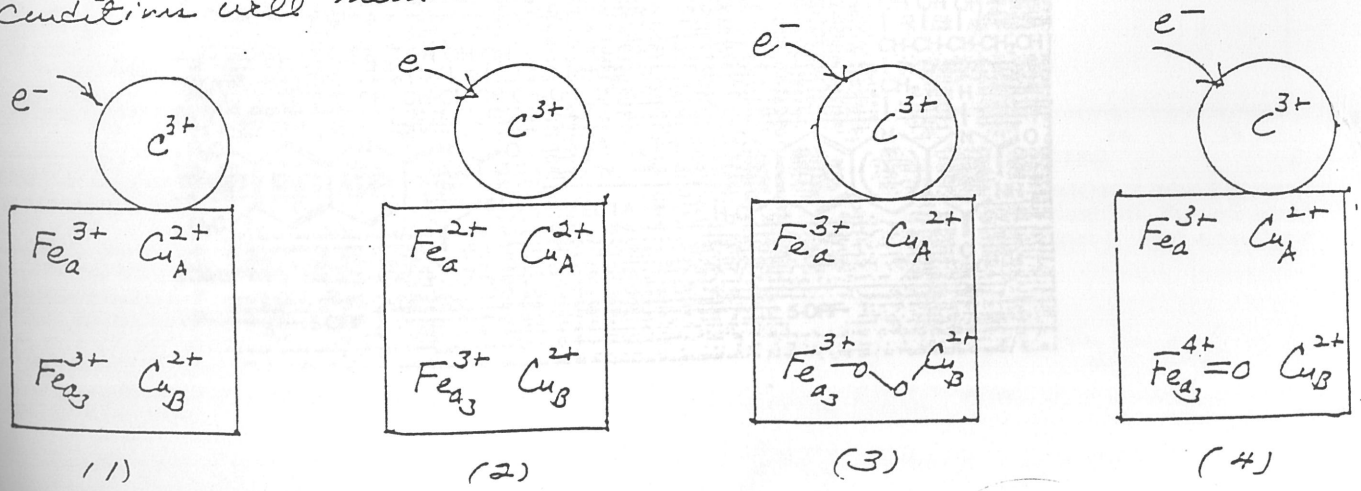

We know that there exists two distinct electron transfer pathways from the low potential redox centers to the dioxygen reduction site. <u>Question</u>: Are the two electron transfer pathways differentially linked to proton pumping? To address this question, we need to follow the electrons into the protein and within the protein in real time under the situations depicted by (1), (2), (3) and (4). No proton pumping is possible in (1) and (2) under aerobic conditions; $2H^+$ are pumped per electron in (3) and (4).

→ Development of a rapid photo initiated reduction of ferricytochrome c

- <u>Photoinitiation</u> because it is easy to "set the clock" using a short laser pulse

* <u>These methods</u> have been developed to carry out such experiments.

(1)

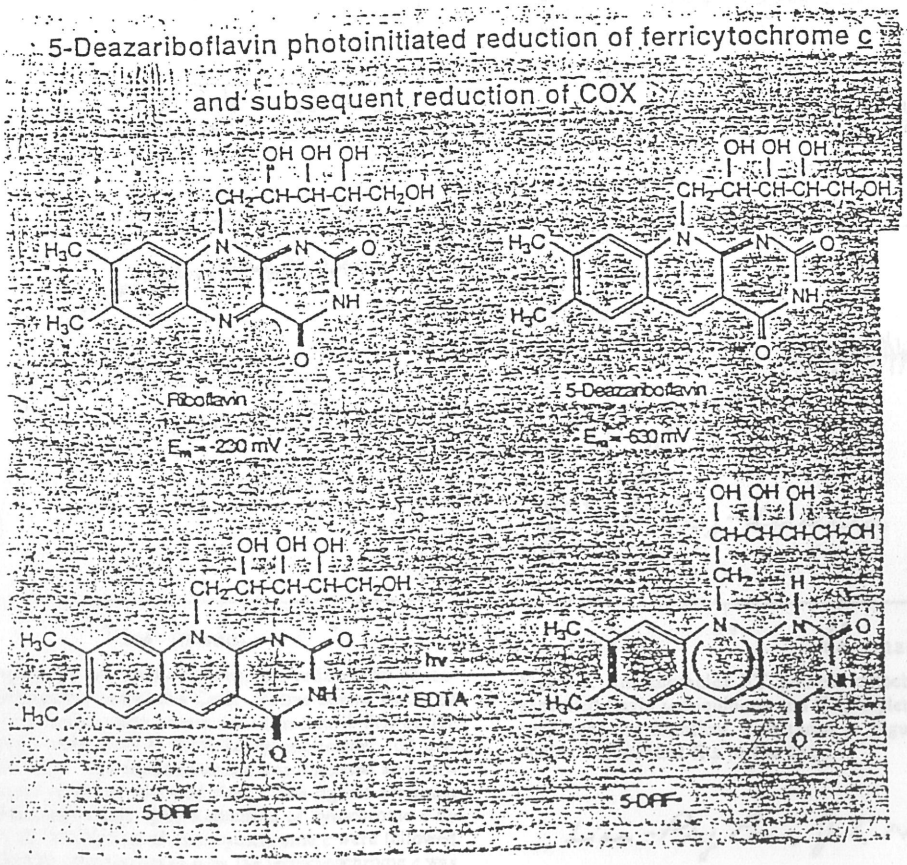

(1) $5\text{-DRF}\cdot + (\text{Cyt}\,\underline{c})_{ox} \xrightarrow{k_1} 5\text{-DRF}_{ox} + (\text{Cyt.}\,c)_{red} + H^+$

(2) $5\text{-DRF}\cdot + (\text{COX})_{ox} \xrightarrow{k_2} 5\text{-DRF}_{ox} + (\text{COX})_{red} + H^+$

(3) $(\text{Cyt.}\,\underline{c})_{red} + (\text{COX})_{ox} \xrightarrow{k_{obs}} (\text{Cyt.}\,\underline{c})_{ox} + (\text{COX})_{red}$

where Cyt $\underline{c}$ ≡ cytochrome $\underline{c}$

COX ≡ cytochrome $\underline{c}$ oxidase

and $k_1 >> k_2$

Ref: Nazzard, J.T.; Rong, S.T.; Tollin, G., Biochem. (1991) 30, 213

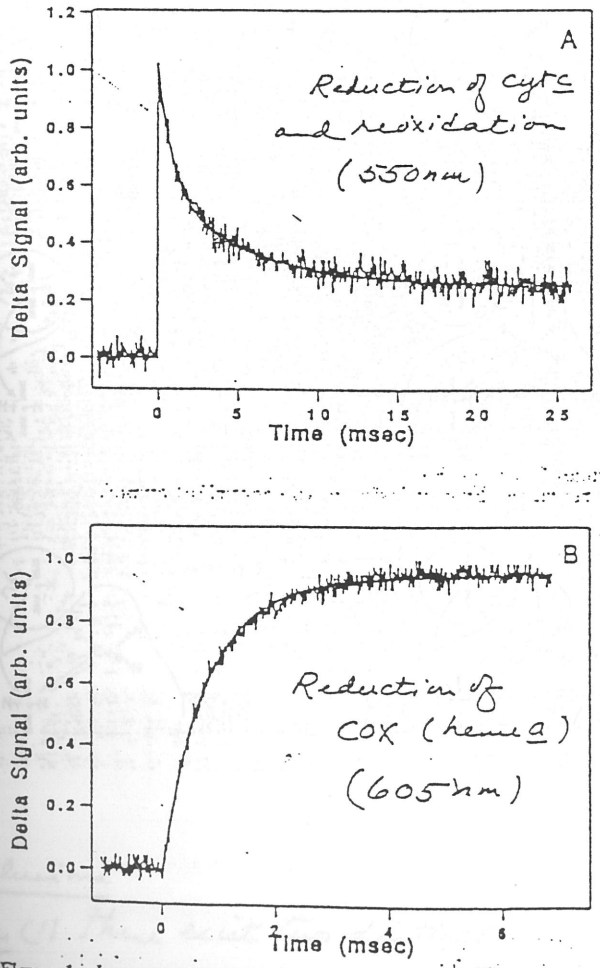

Figure 1. Intracomplex ET between cytochrome *c* reduced by photogenerated flavin semiquinone and native CcO. Native bovine CcO (20 μM) and 20 μM bovine cytochrome *c* were added in 5 mM Tris buffer at pH 7.4 containing 1 mM EDTA, 0.1% lauryl maltoside, 100 μM 5-DRF, and 100 mM KCl. The sample cuvette was degassed and subjected to a N_2 dye laser (BBQ at 390 nm) flash. The signals are sums of four flashes normalized to one. (A) Reduction of cytochrome *c* by flavin semiquinone and reoxidation of ferrocytochrome *c* were followed at 550 nm. (B) Reduction of cytochrome *a* by the ferrocytochrome *c* was observed at 604 nm. Both transients were fitted to a sum of two exponentials (solid curves).

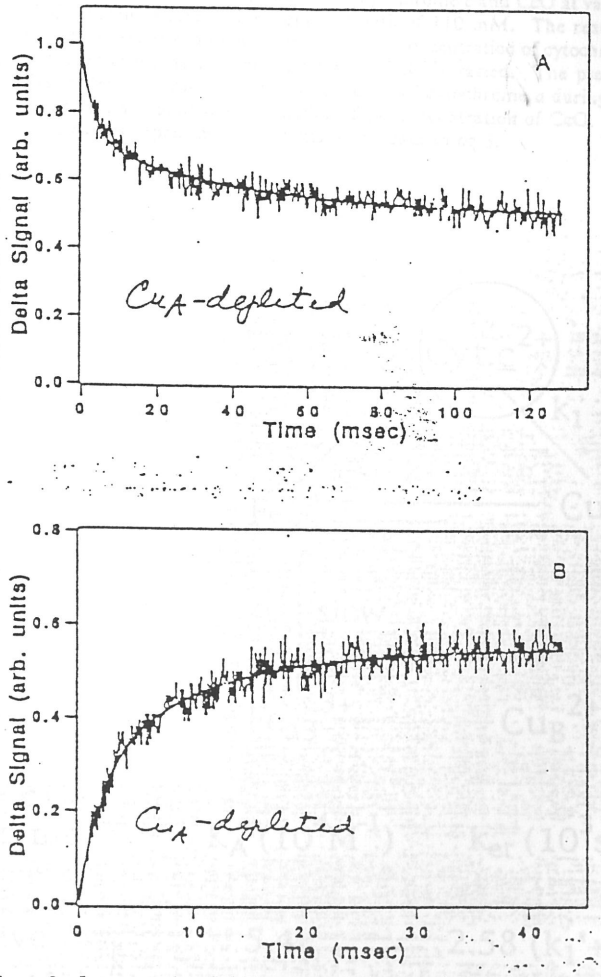

Figure 2. Intracomplex ET between cytochrome *c* reduced by photogenerated flavin semiquinone and Cu_A-depleted CcO. The experimental conditions are identical with those in Figure 1. Solid curves depict double-exponential fits to the data.

Lian-Pin Pan, J.T. Hazzard, Jian Lin, Gordon Tollin and S. I. Chan

JACS (1991) 113, 5908

Electron Input – first electron

$$\text{Cyt } c^{2+} + (\text{CcO})_{ox} \underset{k_2}{\overset{k_1}{\rightleftharpoons}} \text{Cyt } c^{2+}{:}(\text{CcO})_{ox} \qquad (1)$$

$$\text{Cyt } c^{2+}{:}(\text{CcO})_{ox} \xrightarrow[k_{et}]{} \text{Cyt } c^{3+} + (\text{CcO})_{red} \qquad (2)$$

$$k_{obsd} = k_{et}K_A[\text{CcO}]_{ox}/(K_A[\text{CcO}]_{ox} + 1) \qquad (3)$$

where K_A ($= k_1/k_2$), the association constant for the formation of ferrocytochrome c : CcO complex

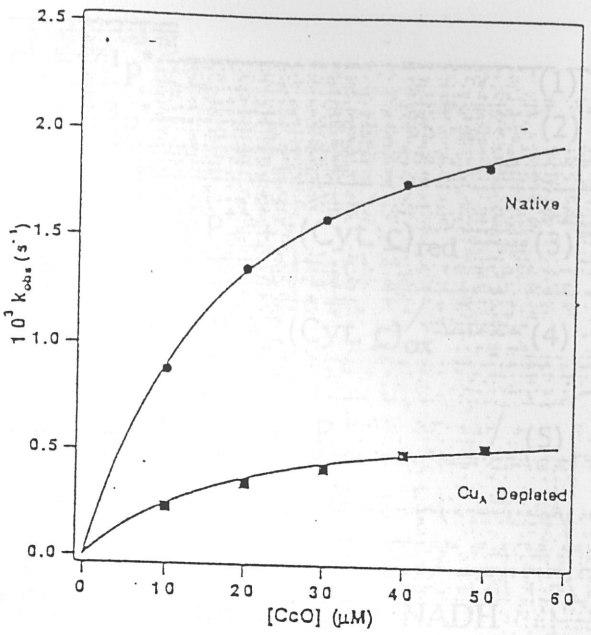

Figure 3. Kinetics of ET between ferrocytochrome *c* and CcO at various CcO concentrations and an ionic strength of 110 mM. The reaction conditions are as shown in Figure 1, and the concentration of cytochrome *c* is unchanged as the concentration of CcO is varied. The pseudo-first-order rate constants for the reduction of cytochrome *a* during the fast phase are plotted as a function of the concentration of CcO. The solid curves represent the best fits of the data to eq 3.

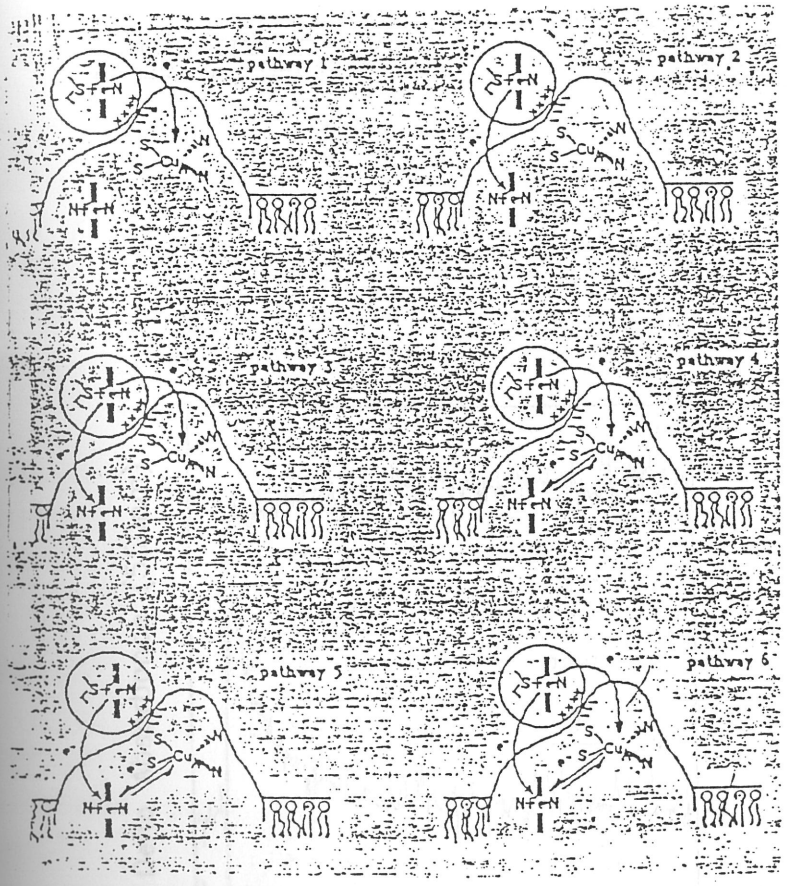

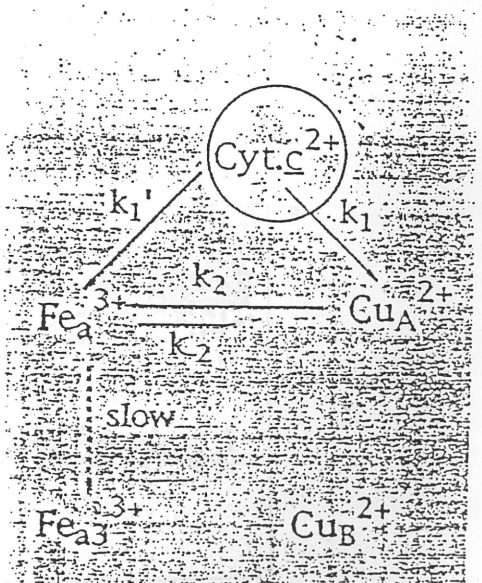

Enzyme	K_A ($10^4 M^{-1}$)	k_{et} ($10^3 s^{-1}$)
Native	5.4	2.58 ($k_1'+k_1$)
Cu_A-depleted	5.0	0.74 (k_1')
Type 1-Cu_A	4.2	2.0 ($k_1'+k_1$)
Type 2-Cu_A	4.0	0.99 (k_1')

$k_2 + k_{-2} = 17{,}000\ s^{-1}$

Conclusions

Either (1) there exist two distinct electron-input ports for ET from ferrocytochrome c to CCO (for 1st electron) with the more facile ET proceeding via Cu_A or Cu_A regulates the rate of direct ET from ferrocytochrome c to cytochrome a

(ii) Uroporphyrin / NADH Photoinitiated Reduction of Ferricytochrome c

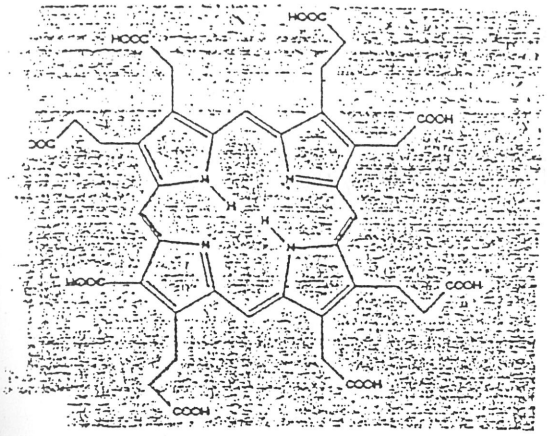

Uroporphyrin (P)

$$P \xrightarrow{h\nu} {}^1P^* \quad (1)$$

$${}^1P^* \longrightarrow {}^3P^* \quad (2)$$

$${}^3P^* + (\text{Cyt. c})_{ox} \longrightarrow P^+ + (\text{Cyt. c})_{red} \quad (3)$$

$$P^+ + (\text{Cyt. c})_{red} \xrightarrow{k_4} P + (\text{Cyt. c})_{ox} \quad (4)$$

$$P^+ + S_{red} \xrightarrow{k_5} S_{ox} + P \quad (5)$$

$$k_4 = 1 \times 10^8\ M^{-1}s^{-1}$$

$$k_5 >> 1 \times 10^8\ M^{-1}s^{-1} \quad \text{for } S_{red} = \text{NADH}$$

R.W. Larsen, J. R. Winkler and S.I. Chan
J. Phys. Chem. (1992)

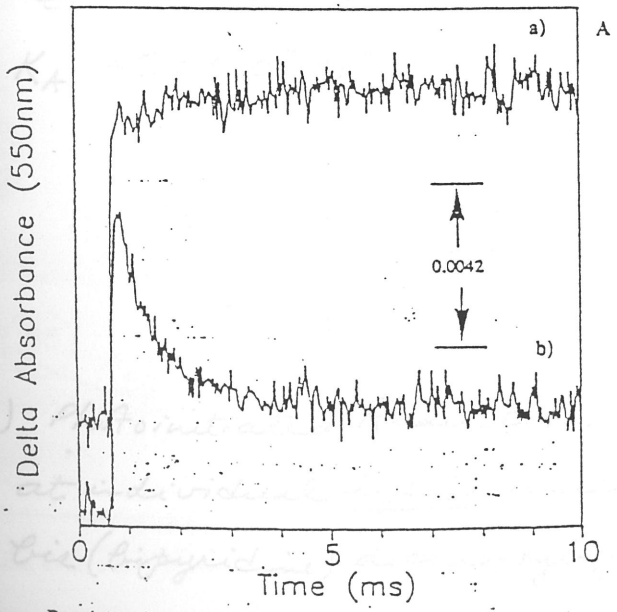

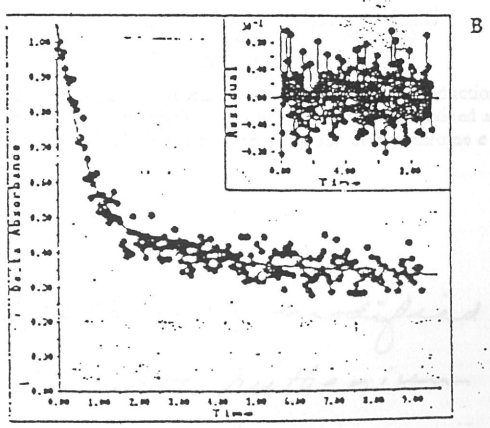

Panel A: absorption transient obtained at 550 nm of a solution containing 15 μM cytochrome c, 15 μM uroporphyrin, and 1 mM NADH in the absence (a) and presence (b) of 15 μM cytochrome c oxidase. Buffer conditions are the same as those in Figure 1. Panel B: double-exponential linear regression analysis of the 550-nm transient of cytochrome c in the presence of cytochrome c oxidase.

↑ Reduction of Ferricytochrome c and Reoxidation via ET to CCO

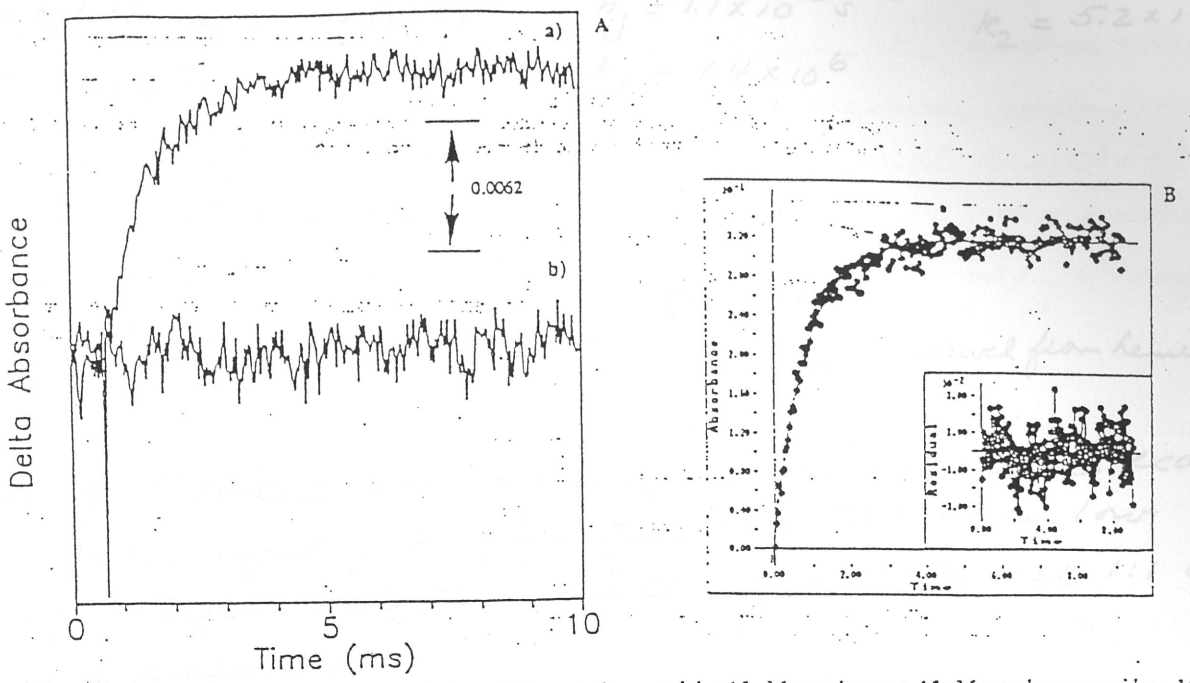

Panel A: absorption transient obtained at 605 nm of (a) a solution containing 15 μM cytochrome *c*, 15 μM cytochrome *c* oxidase, 15 μM uroporphyrin, and 1 mM NADH and (b) 15 μM cytochrome *c* oxidase, 15 μM uroporphyrin, and 1 mM NADH. Buffer conditions are the same as those in Figure 1. Panel B: single-exponential linear regression analysis of the 605-nm transient described in panel A, transient a.

Reduction of heme a in CCO

$k_{ET} = 1829 \pm 248\ s^{-1}$

$K_A = 7.3 \times 10^4\ M^{-1}$

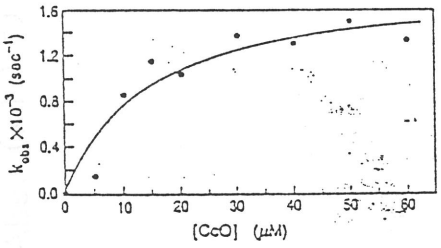

Plot of k_{obs} vs [cytochrome *c* oxidase] for the reduction of cytochrome *a*. The concentration of cytochrome *c* was maintained at 15 μM and titrated with the indicated concentration of cytochrome *c* oxi-

(iii) Photoinitiated Reduction of Cytochrome c modified at individual lysine amino acid with ruthenium bis(bipyridine) dicarboxylbipyridine $[Ru^{II}(bpy)_2(dcbpy)]$

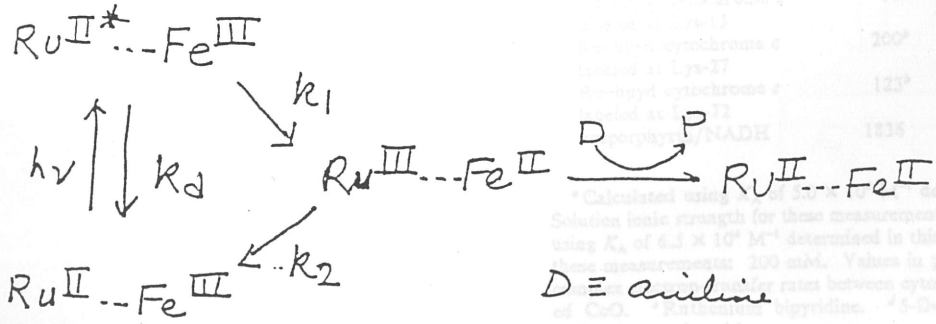

For cytochrome c - modified at lysine 86

$k_d = 1.1 \times 10^6 s^{-1}$ $k_2 = 5.2 \times 10^6 s^{-1}$

$k_1 = 1.4 \times 10^6$

Driving force for ET from Ru^{II*} to Fe^{III} ~ 0.98V

Driving force for reverse ET ~1.05V

Distance 13 Å

(▨) back

(○) front viewed from heme crevice

Recently, F. Millett and coworkers used this approach to examine the electron input of first electron into CCO under low ionic strengths. Under these conditions, $K_A \rightarrow \infty$ and 1:1 cytochrome: CCO is preformed.

$k_{obs} = 3274 s^{-1} \Rightarrow k_{ET}$ (by monitoring 605 nm absorption

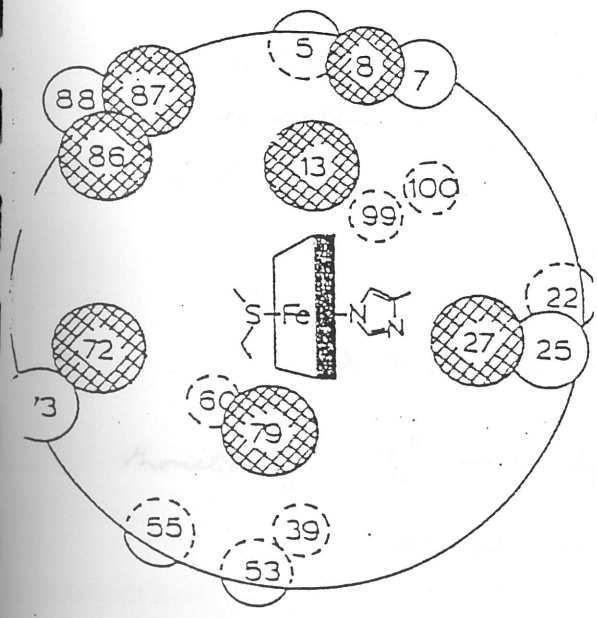

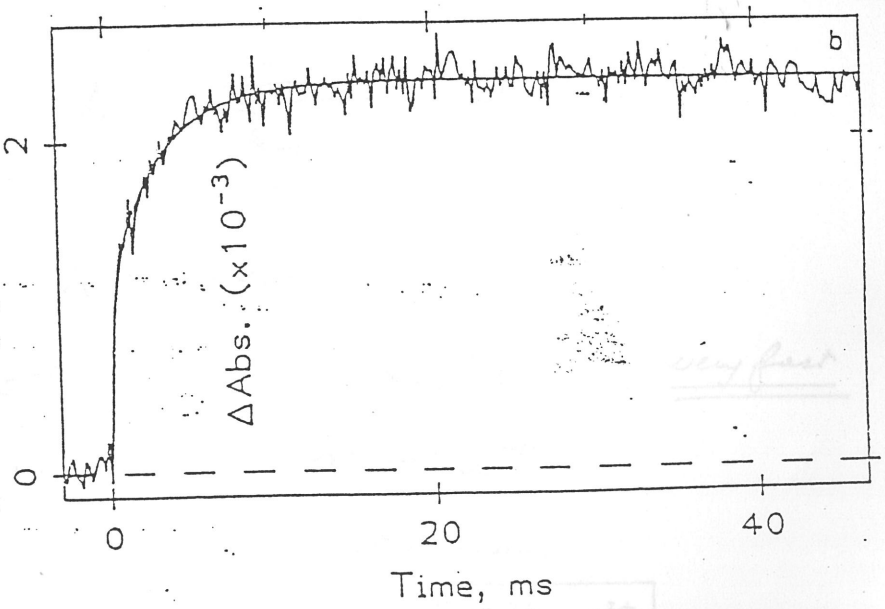

→ Summary of intracomplex electron transfer rates

TABLE I: Summary of Intracomplex Electron-Transfer Rates Using Different Photoreduction Techniques

photoreduction system	intracomplex, electron-transfer rate, s^{-1}	second-order rate constant, $M^{-1} s^{-1}$
5-DRF/EDTA[d]	1470	1.47×10^7 (6)[a]
5-DRF/EDTA	2580 (740)	1.4×10^7 (7)[a] (3.7×10^7)
Ru–bpyd[c] cytochrome *c* labeled at Lys-13	46[b]	0.3×10^7 (8)
Ru–bpyd cytochrome *c* labeled at Lys-27	200[b]	1.3×10^7 (8)
Ru–bpyd cytochrome *c* labeled at Lys-72	123[b]	0.8×10^7 (8)
uroporphyrin/NADH	1836	1.19×10^7 (this work)[b]

[a] Calculated using K_A of $5.0 \times 10^4 M^{-1}$ determined in refs 6 and 7. Solution ionic strength for these measurements: 110 mM. [b] Calculated using K_A of $6.5 \times 10^4 M^{-1}$ determined in this work. Ionic strength for these measurements: 200 mM. Values in parentheses refer to intracomplex electron-transfer rates between cytochrome *c* and Cu_A-depleted CcO. [c] Ruthenium bipyridine. [d] 5-Deazariboflavin/ethylenediaminetetraacetic acid.

Electron input (Second electron)

Difficult to apply above methods to examine the second electron because it is difficult to maintain an appreciable concentration of the 1-electron-reduced enzyme for appreciable lengths of time. The electron eventually redistributes itself among the various metal centers in accordance to their redox potentials. Therefore need another approach.

→ **Perturbed equilibrium experiments**

(a) Two electrons in the protein

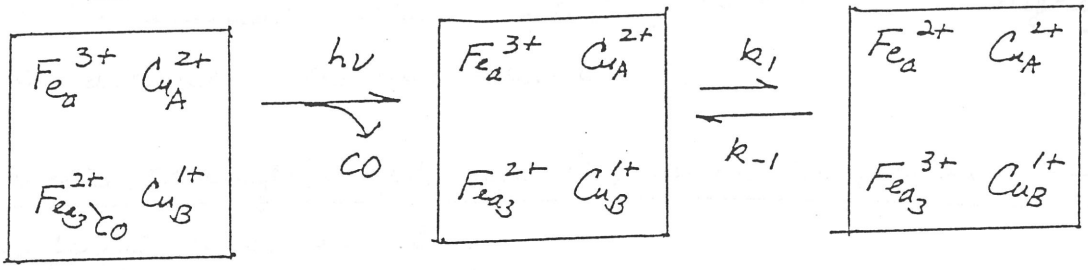

CO-inhibited mixed valent COX

$$A \underset{k_{-1}}{\overset{k_1}{\rightleftharpoons}} B$$

$$\lambda = k_1 + k_{-1}$$

$\lambda = 1.0 \times 10^6\ s^{-1}$ monitoring $a_3^{2+} \longrightarrow a_3^{3+}$ at 444 nm

$1.6 \times 10^6\ s^{-1}$ very fast $a^{3+} \longrightarrow a^{2+}$ at 604 nm

(b) Three electrons in the protein

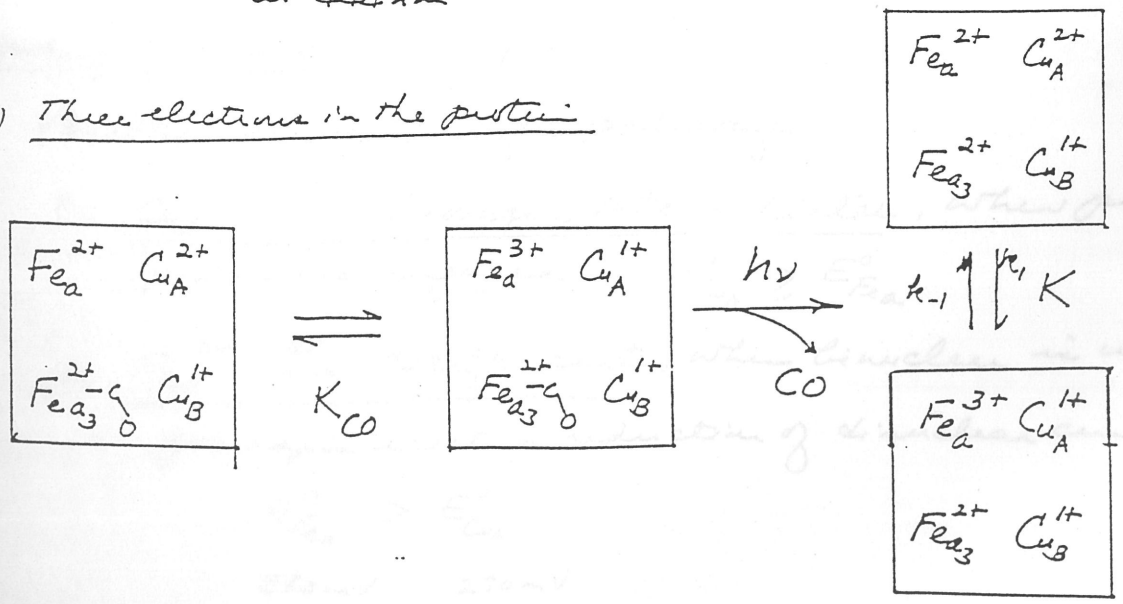

K shifts when CO is off

$$\frac{K}{K_{CO}} \sim 1.02$$

From transient absorption experiments,

following decrease in A_{605} (oxidation of Fe_a^{2+})

decrease in A_{830} (reduction of Cu_A^{2+})

$$k_1 + k_{-1} \sim 17{,}000\ s^{-1}$$

<u>Conclusion from these experiments</u>

Equilibration of electrons among the metal centers is rapid (compared with electron input rate) when there are <u>more than one electron</u> in the protein. Thus, electron leaks will dominate when $[Cyt.\ c^{2+}]$ is high, under highly reducing conditions in the mitochondrion.

→ <u>Electron transfer pathways to reduce the peroxo and oxyferryl intermediates</u>

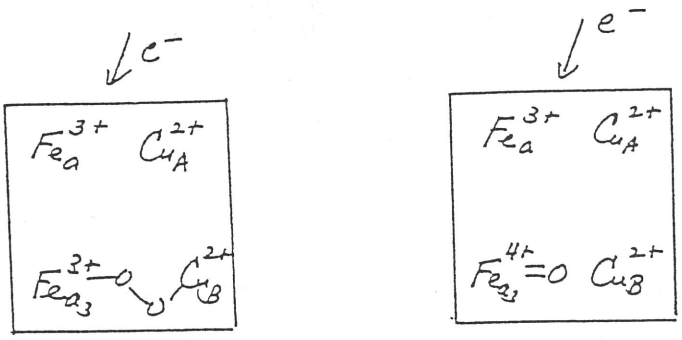

These experiments are still in progress

<u>Working hypothesis</u>

Parallel electron transfer pathways

(1) <u>$Cu_A \xrightarrow{et}$ Dioxygen intermediates</u>, when proton pump is engaged $\quad E^o_{Cu_A} \gtrsim E^o_{Fe_a}$

(2) <u>$Fe_a^{2+} \xrightarrow{et}$ catalytic center</u>, when binuclear is unloaded for rapid electron reduction of binuclear center

$$E^o_{Fe_a} > E^o_{Cu_A}$$

380 mV $\quad$ 270 mV

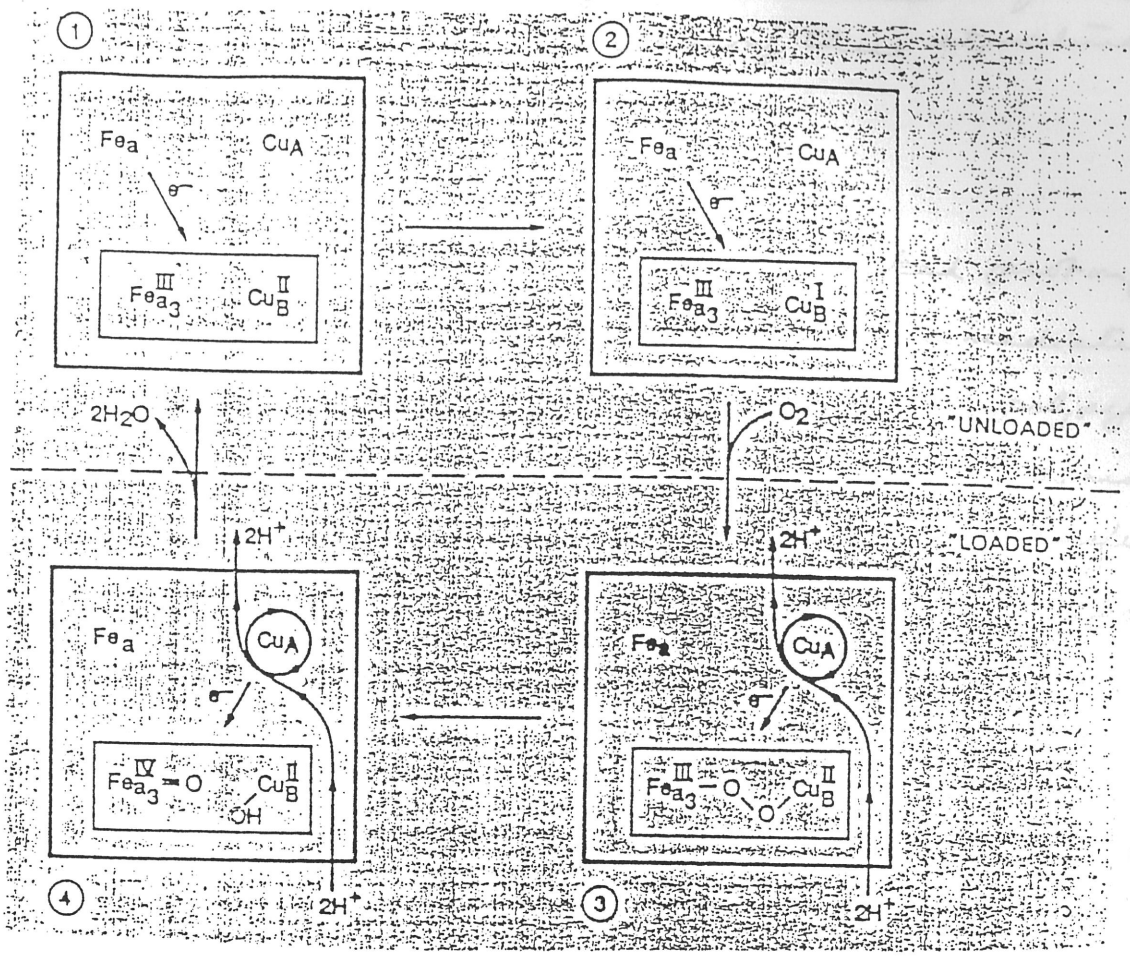

(C) <u>Redox Linkage</u>

Proton pumping → moving H^+ uphill against an electrochemical gradient

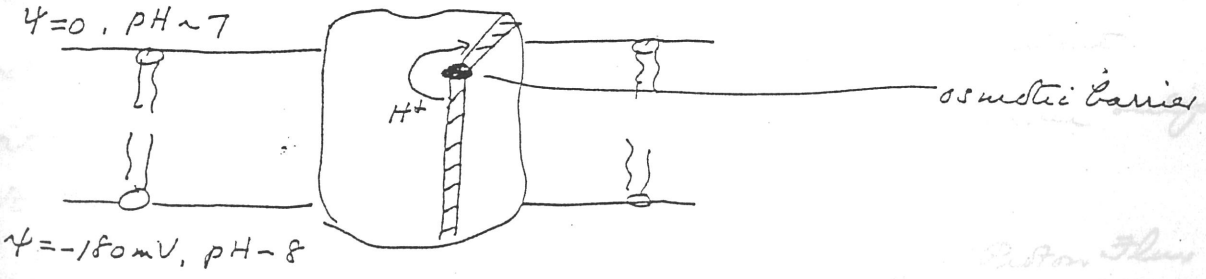

→ CcO is a molecular machine

(1) The functioning of a molecular machine necessitates a source of energy

(2) The molecule exists as a class of structures rather than a single equilibrium structure

(3) The molecule generates according to an ordered sequence of conformational transitions among these structures to achieve kinetic competence.

→ There are three requirements for a redox-linked proton pump.

(1) Redox linkage (There must exist an intermediate wherein redox energy is transmitted to the polypeptide so that two protons are moved across the osmotic barrier just before or during the electron transfer.

(2) Electron gating (for redox linkage to compete effectively against electron leakes) — electron enters redox site at a different protein conformation from that in which the electron is transferred to the acceptor (high-potential dioxygen intermediates)

(3) Proton gating (to avert proton slippage, protons must be taken up in a different protein conformation than that from which they are ejected)

→ Clearly, the proton pumping must be kinetically controlled. Accordingly, part of the free energy available must be dissipated to allow the molecular machine to operate with finite rates. Optimize flux of protons (consistent with electron input flux) to attain maximum power output, not thermodynamic efficiency, i.e.,

Redox energy × Thermodynamic efficiency × Proton Flux

→ <u>A simple picture of redox-linkage</u>

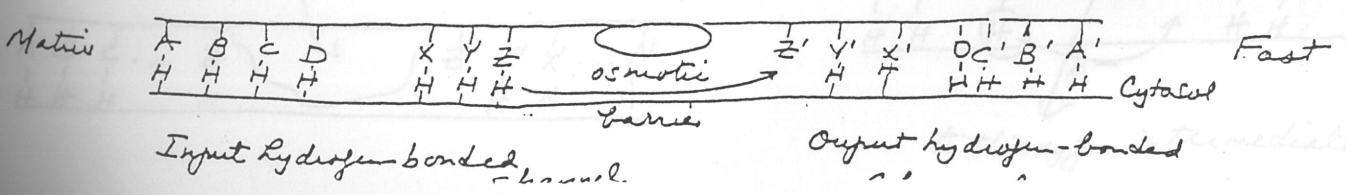

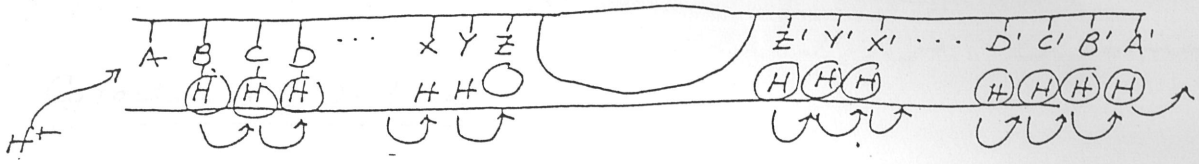

Tandem proton migration forward
proton "hole"

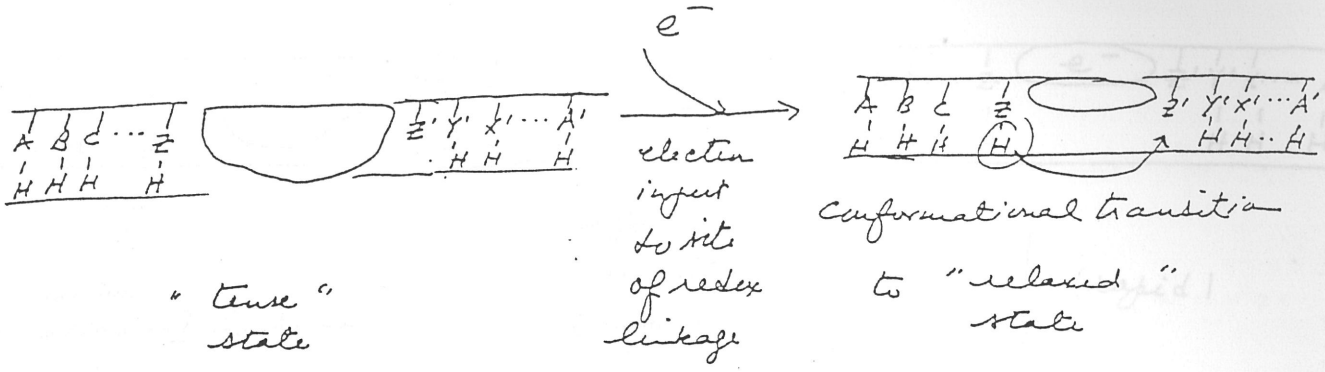

What you see above are some of the elements of proton gating and redox linkage. But electron gating is not so clear here.

If electron reduces the redox center that is the site of linkage without promoting the "tense" → "relaxed" conformational transition indicated above, i.e., the redox center acts passively essentially as a relay to transfer the electron to the dioxygen intermediate(s), then you have an electron leak, or initiated a "futile cycle".

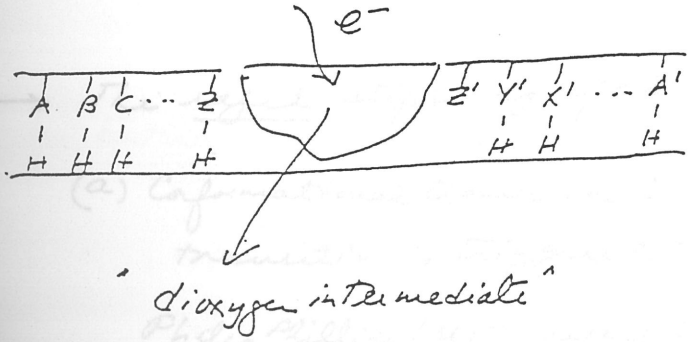

"futile"

To avert "futile" cycle,

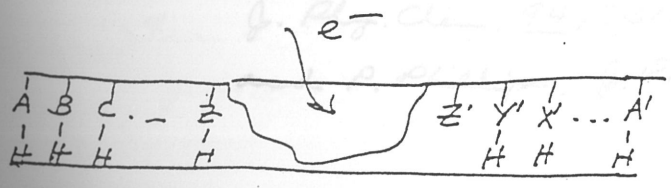

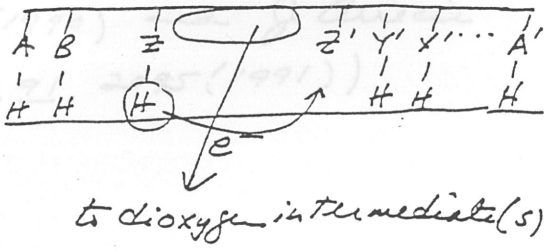

Cytochrome c Oxidase

(C) Redox Linkage (continued)

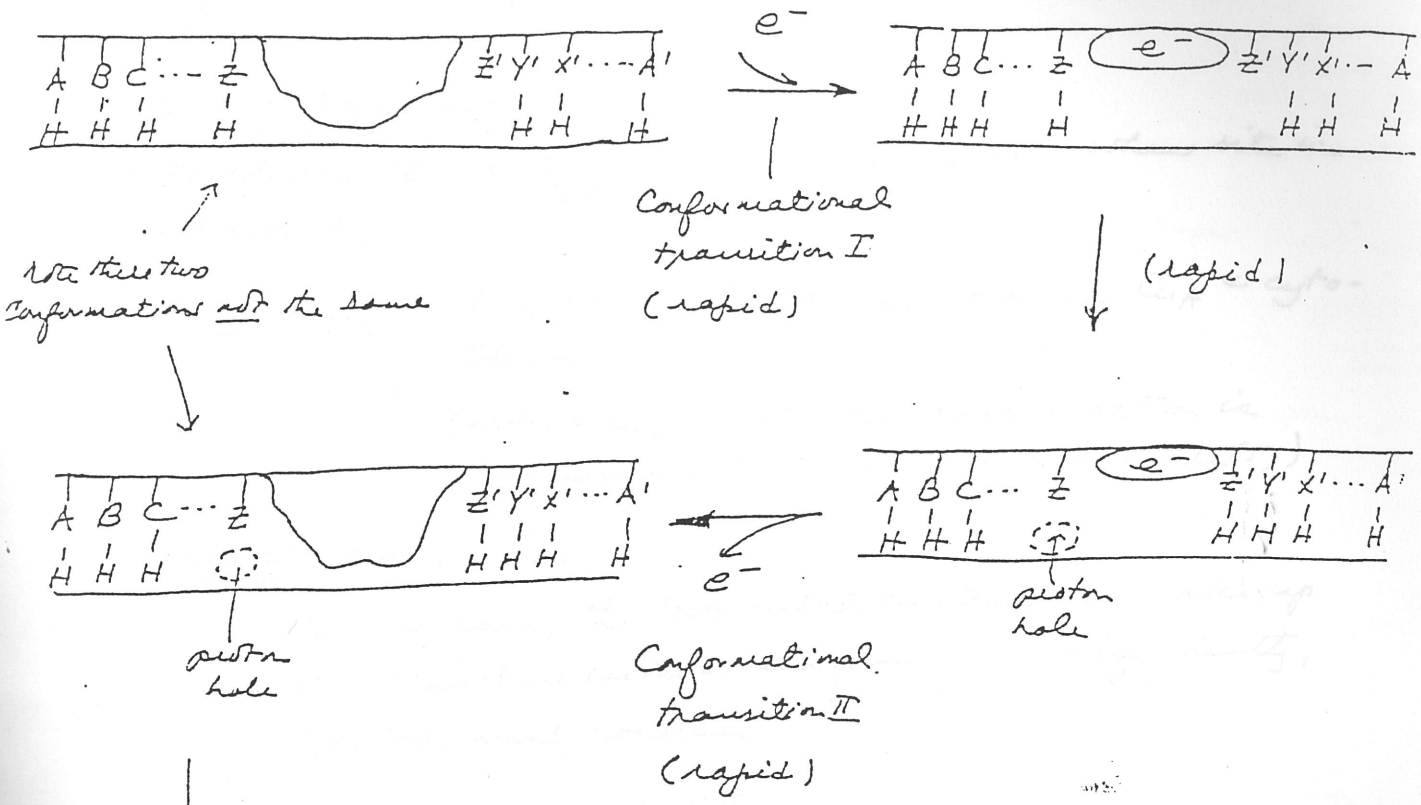

slower steps

(1) ejection of H^+ to "uphill" side of membrane (cytosol)

(2) pick up of H^+ from "downhill" side of membrane (matrix)

→ The rapid steps depicted above constitute redox linkage

(a) Conformational transition I is the triggering step (conformation transition is triggered by e^- reduction of "site of linkage")

Philip Phillips (MIT) refers to this step as "creation of proton ~~pump~~ fault (see J. Arecie, K. Kundu and P. Phillips J. Phy. Chem. 94, 7316-7321 (1990) and J. Arecie and P. Phillips, J. Phys Chem. 91, 2095 (1991))

(b) Note that e^- enters the site of linkage and leaves the site of linkage at a different prot conformation (electron gating)

(c) Note also that the proton crosses the osmotic barrier and the proton hole is replenished in a different protein conformation (proton gating)

→ <u>Site of redox linkage</u>

(the redox center that <u>triggers</u> the redox linkage when site is reduced)

<u>Most likely</u> : low-potential centers, namely Cu_A & cytochrome <u>a</u>

(redox energy dissipated once electron is transferred to dioxygen intermediate(s))

<u>Also proposed</u> : Cu_B

in which case, the two metal centers that make up the binuclear center would function independently, i.e., we must consider

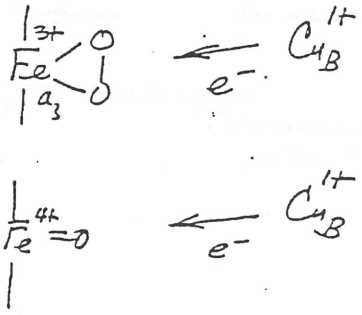

Should be a fairly leaky pump if this is the case, because the two metal centers are very close

<u>Entirely reasonable</u> : that the binuclear site and one of the low-potential redox centers work in concert to achieve redox linkage. After all, the binuclear site must be activated by O_2 binding for proton pumping to occur

From the point of energetics, we can illustrate the two possibilities this way

Case a : Low-potential center acting essentially alone as site of redox linkage

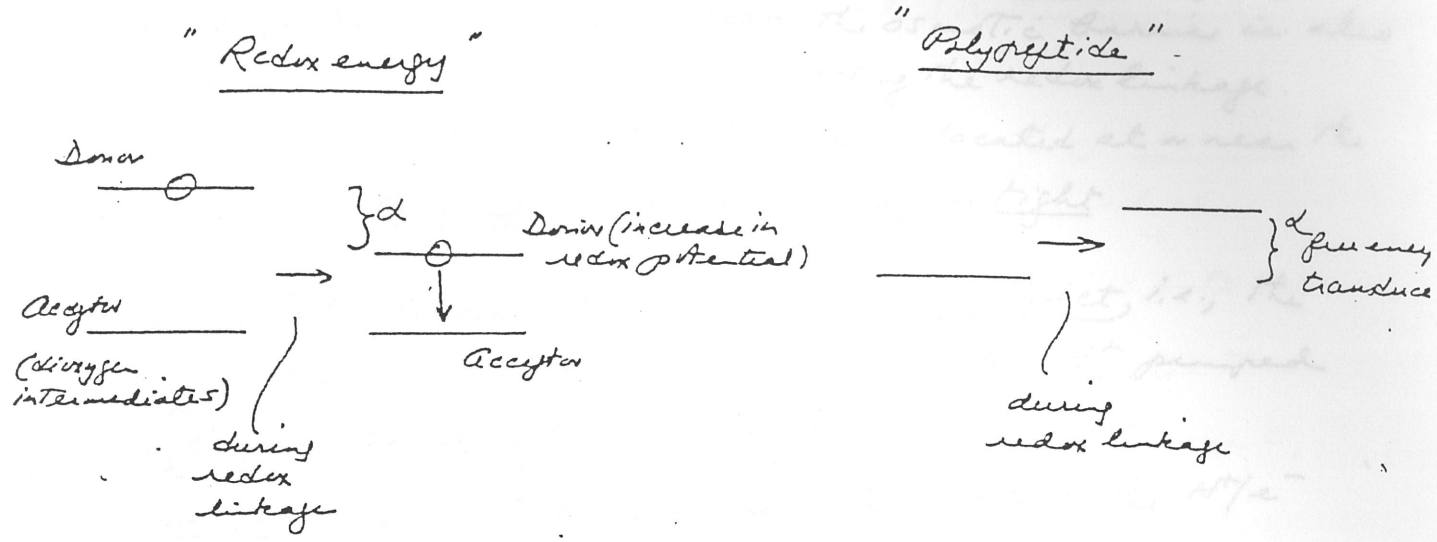

Case b : Low potential center working together with dioxygen intermediates to achieve redox linkage

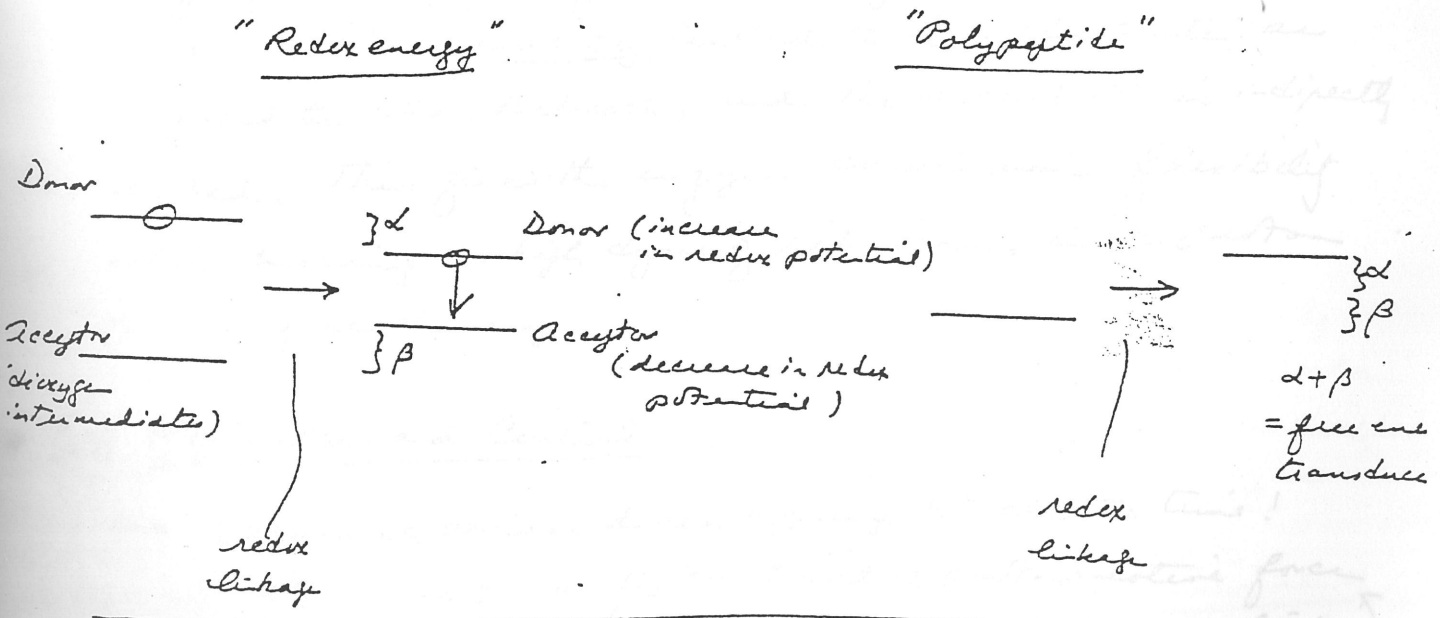

If $\alpha \gg \beta$, we have case a ; the low potential center is truly the site of linkage

If $\alpha \ll \beta$, then the dioxygen intermediates (not heme a_3 or Cu_B) are primarily responsible for coupling redox energy to the polypeptide.

Case a seems more likely, since one of the dioxygen intermediates is an oxyferryl and this species is relatively insulated structurally

→ Direct coupling vs Indirect coupling

Both the Babcock and Chan models assume direct coupling, i.e., the proton that is moved across the osmotic barrier is also part of the redox center that is directing the redox linkage. In other words, the osmotic barrier is located at or near the redox center. Advantage: e^-/H^+ linkage is tight

But the redox linkage could also be indirect, i.e., the proton channels and osmotic barrier for the H^+ pumped is only conformationally linked to the redox center.

Advantage: e^-/H^+ linkage is not tight, so that the H^+/e^- stoichiometry can be readily ~~controlled~~ varied.

In fact, since $2H^+$ are pumped per electron during each step of the second half of the catalytic cycle, it is possible that $1\ H^+$ is directly linked to the redox center as proposed by Chan, Babcock, and the second H^+ is indirectly linked. This gives the enzyme considerable flexibility while ensuring a high degree of robustness in its proton pumping machinery.

• (D) Regulation and Control

→ Cytochrome c oxidase doesn't pump H^+ all the time!
$H^+/e^- \rightarrow 0$ as the counteracting protomotive force becomes too high and when [ATP]/[ADP] becomes high.

ΔpH
$\Delta\psi$

→ Mechanisms of control

(a) $\Delta\psi$: coupled electron transfers (& hence redox linkage) slow down and electron leaks take over

(b) ΔpH: proton slippage or backflow

(c) ATP : (i) Negative feedback

Mammalian oxidase has an ATP binding machinery (subunit IV) ← Mg^{2+} is located in this subunit

(ii) Positive feedback

There appear to be two cytochrome c's for P. aeruginosa denitrificans CcO; one cytochrome c_{552}, which is membrane-bound and shuttles electrons into CcO via cytochrome a; the other, cytochrome c_{550}, is water-soluble, just like mammalian cytochrome c, and it transfers its electron into CcO via Cu_A. Under low [ATP] levels, the bacteria grows by metabolizing different substrates other than succinate, e.g. CH_3OH and CH_3NH_2, and expresses a totally different set of genes including one for the water-soluble c_{550}.

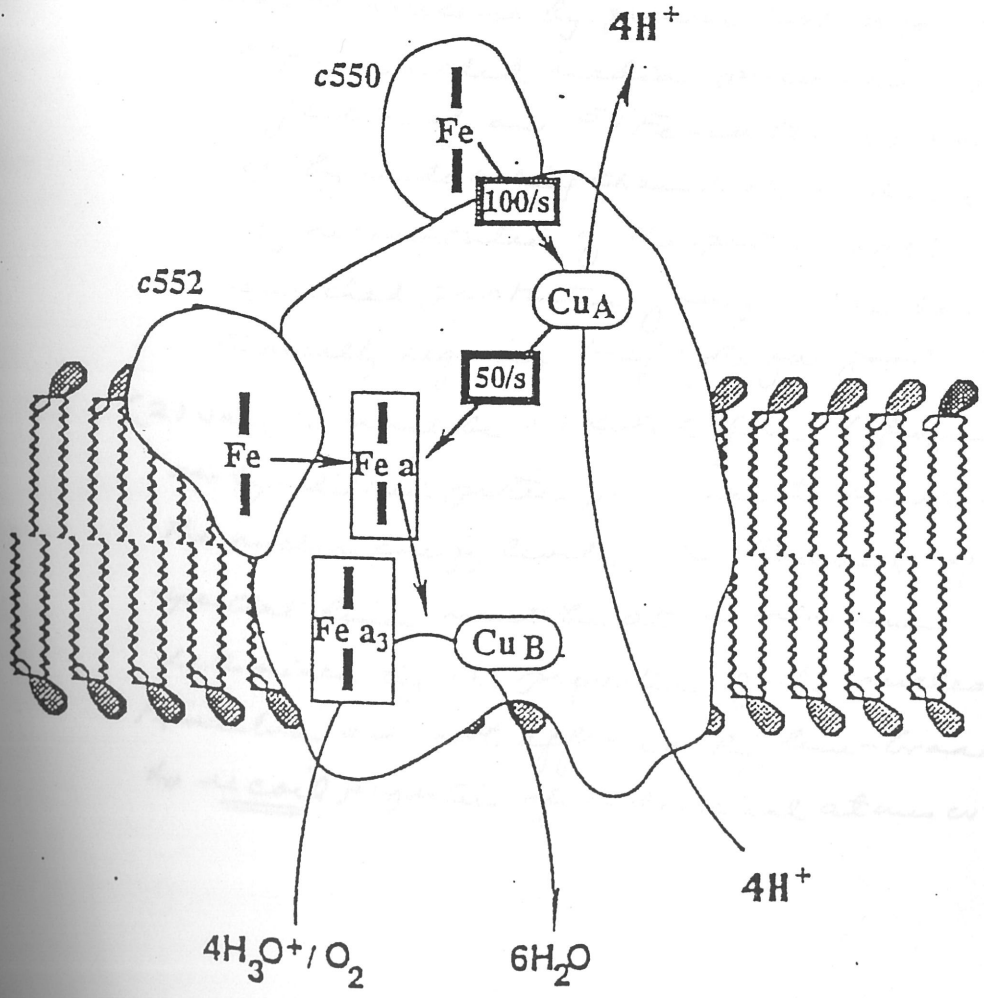

The implication here is that the two electron inputs are differentially coupled to vectorial proton translocation. If so, Cu_A → dioxygen intermediate(s) electron transfer must be linked to proton pumping.

Mössbauer Spectroscopy (Ref A. J. Bearden and W. R. Dunham in "Structure & Bonding" Vol. 8 (1970) pp 1–52)

→ Nuclear γ-ray resonance spectroscopy

→ measures small changes in the nuclear energy levels of a suitable Mössbauer nuclide produced by the interactions of the nuclide with the electronic surroundings

→ The most important Mössbauer nuclide for biochemical studies is ^{57}Fe : ^{57}Fe Mössbauer spectroscopy is one of the most important spectroscopic tools to elucidate the electronic configurations at iron nuclei in iron-containing proteins

→ Attractive features:

(1) No interfering signals from other atomic species.

(2) The Mössbauer nuclide does not perturb the protein from its normal configuration

→ Disadvantages:

(1) Low natural abundance of the ^{57}Fe nuclide (2.19%) (may be overcome by growing host organism on an ^{57}Fe-enriched media, pulse-enrichment by injection of an ^{57}Fe-containing metabolite; or by undertaking chemical exchange directly or by reconstitution of the protein with an ^{57}Fe enriched prosthetic group. Mössbauer spectroscopy typically requires 1–2 μmole for good S/N

(2) Sample must be in solid form (frozen solution or lyophilized protein). To see the small changes in the nuclear energy levels, the linewidths of the Mössbauer spectral lines must be at a minimum and determined by the properties of the nuclear transition themselves and not affected by line-broadening due to recoil properties of individual atoms or molecules!

The Mössbauer Experiment

→ Requirements

(1) Source of γ-rays : ^{57}Co (5–60 mCi)

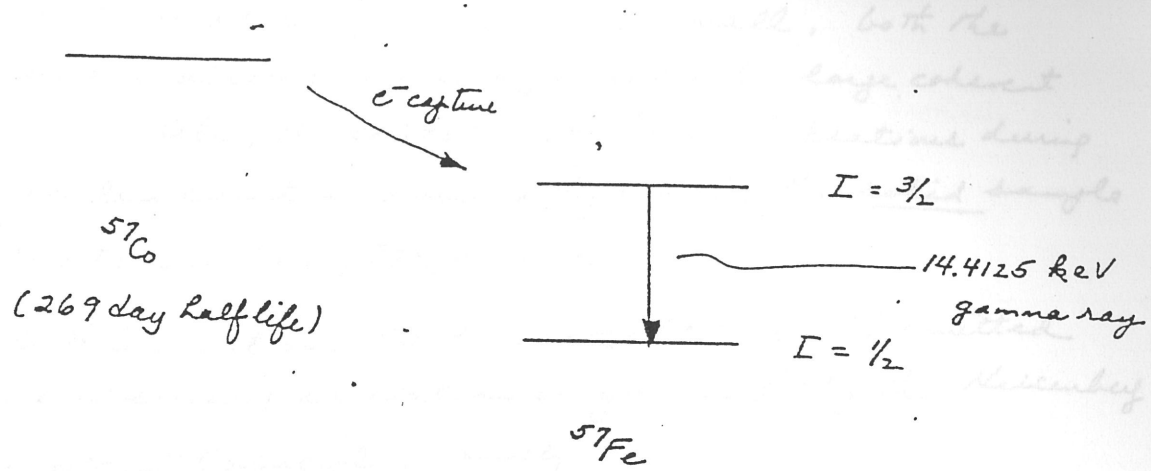

(2) Absorber containing the Mössbauer nuclide (^{57}Fe enriched protein)

(3) Proportional counter or scintillation counter as a detector of radiation (14.4 keV gamma rays)

(4) A transducer to move the source relative to the absorber so that the energy of the incident radiation can be shifted by the first-order doppler shift: $\frac{\delta E}{E_0} = \frac{v}{c}$, where v is the relative velocity between the source and absorber, and E_0 is the energy of the Mössbauer transition (14.4 ke

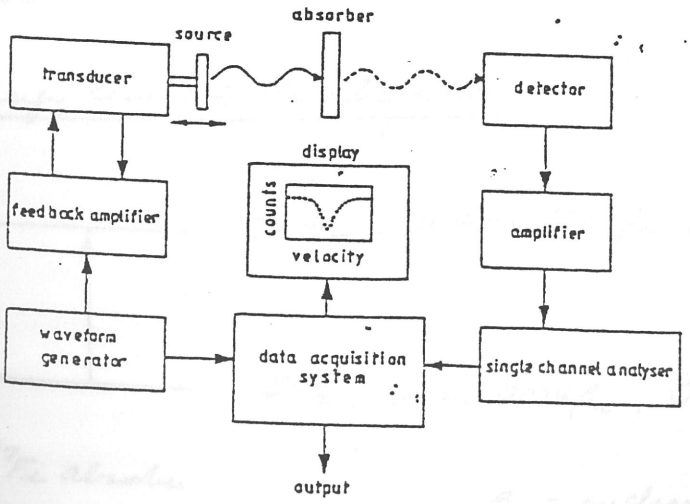

Block diagram of a typical Mössbauer spectrometer

Absorbance is recorded as a function of v, and hence $\frac{\delta E}{E_0} \cdot c$

For the 14.4125 keV transition of ^{57}Fe,

$$1 \text{ mm/s} = 4.8075 \times 10^{-8} \text{ eV} = 3.8776 \times 10^{-4} \text{ cm}^{-1}$$
$$= 11.625 \text{ MHz}$$

(5) To render recoil energies vanishing small, both the source and absorber are incorporated into large coherent masses. Also, the excitation of lattice vibrations during the nuclear event is averted by cooling the <u>solid</u> sample to low temperatures, 77K or lower.

Under these conditions, the linewidths (ΔE) of the emitted (and absorbed) radiation is governed by the Heisenberg Uncertainty Principle, namely

$$\Delta E = h/2\pi\tau$$

where τ is the mean lifetime of the nuclear state. $\tau = 1.4 \times 10^{-7}$ sec for the first excited state of ^{57}Fe, and this correspond to an energy width of 10^{-9} eV. The fullwidth at one-half maximum for an "unsplit" source/absorber combination is ~0.2 mm/s. The effects of the electronic configurations surrounding the Fe nuclide on the energies of the nuclear states/levels are typically 10–100 times the natural linewidth.

- <u>The energy levels of the absorber</u>

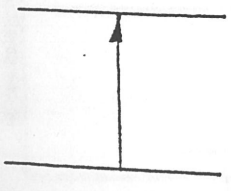

$I = 3/2$, $\mu = -0.1547\,\beta_n$, $Q = 0.3$ barns

$I = \frac{1}{2}$, $\mu = 0.9024\,\beta_n$, $Q = 0$

^{57}Fe absorber

$\beta_n \equiv$ nuclear magneton

The energy levels of the ground and excited nuclear states are differentially modulated by interactions of the nuclide with the electronic surroundings via the different magnetic and electric properties of the nuclide in the two states. The important interactions are

(1) the nuclear isomer (chemical) shift;
(2) the nuclear electric-quadrupole interaction when the nuclide is in the excited state;
(3) the nuclear hyperfine interaction
(4) the nuclear Zeeman interaction in the presence of an external magnetic field $\vec{B}$

→ (1) <u>The nuclear isomer shift</u>

The isomer shift is brought about by small changes in the nuclear energy levels in both the source and absorber due to electrostatic monopole interaction between the charged nuclide and charge density of the electrons at the nuclear position.

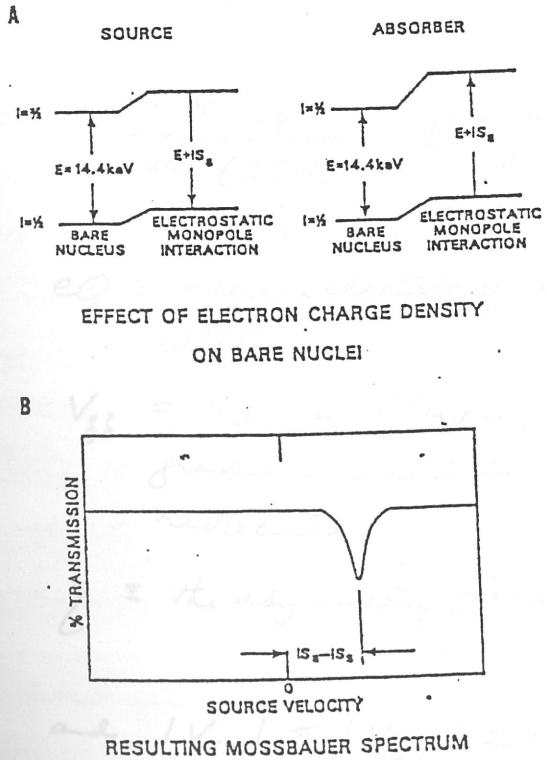

Fig. 1. Mössbauer spectrum resulting from nuclear isomer shift

Only the differences in the interactions between the excited and ground nuclear states and between the source and absorber is measured.

Accordingly, isomer shifts are referred to a "standard" absorber, usually Fe metal. When $\delta^*(X)$ denotes the isomer shift of the <u>sample</u> wrt to a <u>source</u> in matrix X, the isomer shift $\delta(\alpha\text{-Fe})$ wrt α-Fe at RT is given by

$$\delta(\alpha\text{-Fe}) = \delta^*(X) + \delta_s(X)$$

where $\delta_s(X) = +0.349$ mm/s for Pt = X; $+0.225$ mm/s for Cu;

$\delta_s(X) = +0.106$ mm/s for $X \equiv Rh$; $+0.177$ mm/s for $X \equiv Pd$.

Isomer shifts are highly dependent on the details of the electronic configuration; e.g.,

$\delta(\alpha\text{-Fe}) = +0.90 - 1.30$ mm/s (1–2 mm/s) for ferrous high-spin iron

$+0.35 - 0.60$ mm/s for ferric high-spin iron

$+0.05 - 0.10$ mm/s for oxyferryl (Fe(IV))

~ 0.30 mm/s for both low-spin ferric and ferrous iron.

→ (2) <u>The nuclear-electric quadrupole interaction</u>

The $I = 3/2$ excited isomeric state of ^{57}Fe has a quadrupole moment of 0.2 barns, which can interact with the electric field gradient of the electron cloud.

Interaction is described by

$$\frac{eQ\,V_{zz}}{4I(2I-1)} \cdot \left[3I_z^2 - I(I+1) + \eta\left(I_x^2 - I_y^2\right)\right]$$

$eQ \equiv$ nuclear-electric quadrupole moment of the excited state,

V_{zz} = the main (largest) component of the electric field gradient tensor in the principal axis system of the molecule.

$\eta \equiv$ the asymmetry parameter $\equiv \dfrac{V_{xx} - V_{yy}}{V_{zz}}$

and $|V_{xx}| \leq |V_{yy}| \leq |V_{zz}|$

For the ground nuclear state, $I = 1/2$, $Q = 0$, and there is no nuclear electric quadrupole interaction, even though the electric field tensor (namely V_{xx}, V_{yy}, V_{zz}) same as for excited isomeric state

<u>High-spin Fe(II)</u>

large q, and hence large $QS \equiv$ quadrupole splitting

$QS \sim 2-4$ mm/s

<u>High-spin Fe(III)</u>

small q, and hence small QS (0.6-1.0 mm/s)

(Reason: electron cloud due to d-electrons → spherically symmetric in the free ion limit in either O_h or T_d ligand fields)

and for hence

$QS \sim \pm 2$ mm/s

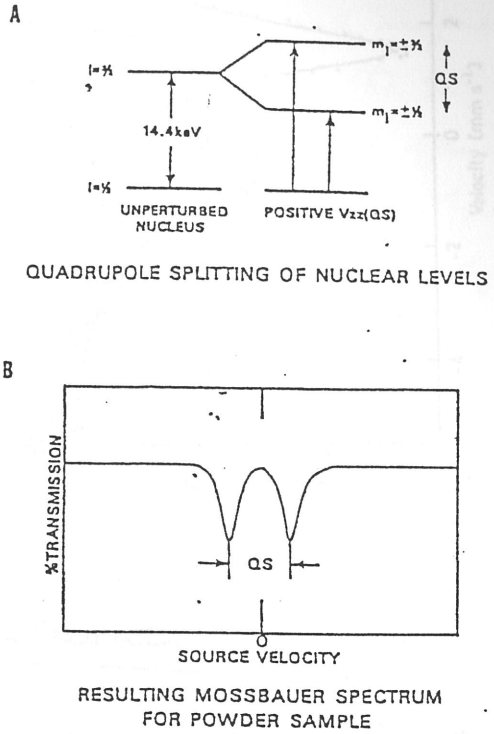

Fig. 2. Mössbauer spectrum resulting from nonzero electric field gradient at the Mössbauer nuclear position for a powder sample

Because of nuclear electric quadrupole interaction, the nuclear spin levels of excited state is split into $m_I = \pm 1/2$ and $m_I = \pm 3/2$ levels, and the Mössbauer spectrum consists of two lines displaced from the position determined by the isomeric shift.

<u>Note</u> that high-spin Fe(II) is usually recognized in Mössbauer spectroscopy by <u>large values</u> of the <u>isomer shift</u> (1-2 mm/s) and the <u>quadrupole splitting</u> (2-4 mm/s)

Low-spin Fe(II), high spin Fe(III) and low spin Fe(III) exhibit comparable isomer shifts and QS, namely relatively small values of δ and QS.

Mössbauer spectrum of high-spin Fe(III) porphyrin m
$\delta(\alpha\text{-Fe}) = +0.43$ mm/s and $QS = \Delta E_Q = +2.2$ m

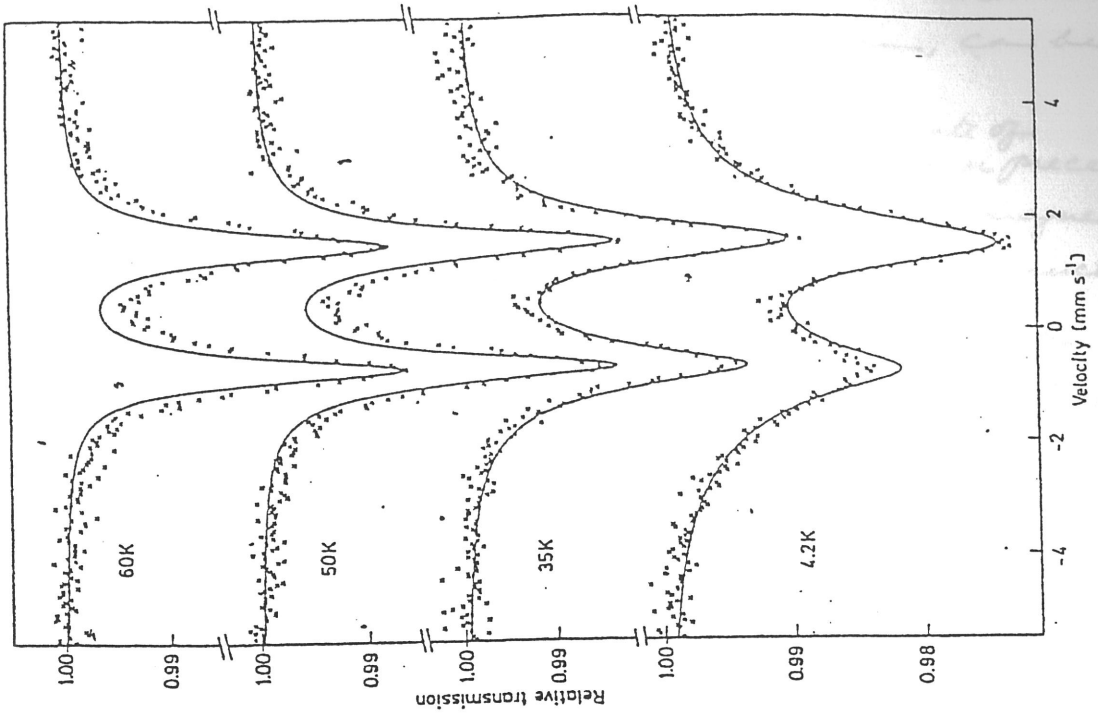

Mössbauer spectra of a (trifiato)(aquo)porphyrinato-iron(III) complex recorded at temperatures ranging from 4.2 K to 60 K in an applied field of 12 mT perpendicular to the γ rays. The *solid lines* represent the simulations based on spin (S = 5/2) Hamiltonian, Eq. (1), taking into account spin–spin relaxation with a relaxation constant $w^{ss} = 4.4 \times 10^7$ rad s^{-1} for the 4.2 K spectrum and spin–lattice relaxation with $w^{sl} = 9 \times 10^3$ rad s^{-1} K^{-1} for the other spectra. Parameters used: $\delta(\alpha\text{-Fe}) = 0.43$ mm s^{-1}, $\Delta E_Q = +2.2$ mm s^{-1}, $\eta = 0$, $g_\perp = 1.9$, $g_\parallel = 2.0$, $A_\parallel/g_n\beta_n = -13.5$ T, $A_\perp/g_n\beta_n = -17$ T, $E = 0$ cm^{-1}, and $D = 15.6$ cm^{-1}

→ (3) <u>The nuclear hyperfine interaction</u>

$$\mathcal{H}_{\substack{\text{hyperfine}\\ \text{interaction}}} = \langle S \rangle \cdot \underset{\sim}{A} \cdot \vec{I} = -g_N \beta_N \vec{H}_{el} \cdot \vec{I}$$

$$\text{or } \vec{H}_{el} = -\frac{\langle S \rangle \cdot A}{g_N \beta_N}$$

These internal magnetic fields experienced by the nuclide can be quite large ~ 500–600 kOe for the fine unpaired electrons in the $^6S_{5/2}$ state of Fe(III) ion (cf 300 kOe for the internal field produced in Fe metal, a ferromagnet)

<u>Observation of a nuclear hyperfine field is positive identification of electron paramagnetism with the paramagnetism located close to the Mössbauer nuclide.</u>

i.e., $\langle S \rangle \neq 0$ and $\underset{\sim}{A} \neq 0$